

EXPLORING KEPLER GIANT PLANETS IN THE HABITABLE ZONE

MICHELLE L. HILL,^{1,2,3} STEPHEN R. KANE,^{4,1} EDUARDO SEPERUELO DUARTE,⁵ RAVI K. KOPPARAPU,^{6,7,8}
DAWN M. GELINO,⁹ AND ROBERT A. WITTENMYER¹

¹*University of Southern Queensland, Computational Engineering and Science Research Centre, Toowoomba, Queensland 4350, Australia*

²*University of New England, Department of Physics, Armidale, NSW 2351, Australia*

³*San Francisco State University, Department of Physics & Astronomy, 1600 Holloway Avenue, San Francisco, CA 94132, USA*

⁴*University of California, Riverside, Department of Earth Sciences, CA 92521, USA*

⁵*Instituto Federal do Rio de Janeiro, Grupo de Física e Astronomia, R. Cel. Delio Menezes Porto, 1045, CEP 26530-060, Nilópolis - RJ, Brazil*

⁶*NASA Goddard Space Flight Center, 8800 Greenbelt Road, Mail Stop 699.0 Building 34, Greenbelt, MD 20771*

⁷*NASA Astrobiology Institutes Virtual Planetary Laboratory, P.O. Box 351580, Seattle, WA 98195, USA*

⁸*Sellers Exoplanet Environments Collaboration, NASA Goddard Space Flight Center.*

⁹*NASA Exoplanet Science Institute, Caltech, MS 100-22, 770 South Wilson Avenue, Pasadena, CA 91125, USA*

ABSTRACT

The *Kepler* mission found hundreds of planet candidates within the Habitable Zones (HZ) of their host star, including over 70 candidates with radii larger than 3 Earth radii (R_{\oplus}) within the optimistic HZ (OHZ) (Kane et al. 2016). These giant planets are potential hosts to large terrestrial satellites (or exomoons) which would also exist in the HZ. We calculate the occurrence rates of giant planets ($R_p = 3.0\text{--}25 R_{\oplus}$) in the OHZ and find a frequency of $(6.5 \pm 1.9)\%$ for G stars, $(11.5 \pm 3.1)\%$ for K stars, and $(6 \pm 6)\%$ for M stars. We compare this with previously estimated occurrence rates of terrestrial planets in the HZ of G, K and M stars and find that if each giant planet has one large terrestrial moon then these moons are less likely to exist in the HZ than terrestrial planets. However, if each giant planet holds more than one moon, then the occurrence rates of moons in the HZ would be comparable to that of terrestrial planets, and could potentially exceed them. We estimate the mass of each planet candidate using the mass-radius relationship developed by Chen & Kipping (2016). We calculate the Hill radius of each planet to determine the area of influence of the planet in which any attached moon may reside, then calculate the estimated angular separation of the moon and planet for future imaging missions. Finally, we estimate the radial velocity semi-amplitudes of each planet for use in follow up observations.

Keywords: astrobiology – astronomical databases: miscellaneous – planetary systems – techniques: photometric, radial velocity, imaging

1. INTRODUCTION

The search for exoplanets has progressed greatly in the last 3 decades and the number of confirmed planets continues to grow steadily. These planets orbiting stars outside our solar system have already provided clues to many of the questions regarding the origin and prevalence of life. They have provided further understanding of the formation and evolution of the planets within our solar system, and influenced an escalation in the area of research into what constitutes a habitable planet that could support life. With the launch of NASA’s *Kepler* telescope thousands of planets were found, in particular planets as far out from their host star as the Habitable Zone (HZ) of that star were found, the HZ being defined as the region around a star where water can exist in a liquid state on the surface of a planet with sufficient atmospheric pressure (Kasting et al. 1993). The HZ can further be divided into two regions called the conservative HZ (CHZ) and the optimistic HZ (OHZ) (Kane et al. 2016). The CHZ inner edge consists of the runaway greenhouse limit, where a chemical breakdown of water molecules by photons from the sun will allow the now free hydrogen atoms to escape into space, drying out the planet at 0.99 AU in our solar system (Kopparapu et al. 2014). The CHZ outer edge consists of the maximum greenhouse effect, at 1.7 AU in our solar system, where the temperature on the planet drops to a point where CO₂ will condense permanently, which will in turn increase the planet’s albedo, thus cooling the planet’s surface to a point where all water is frozen (Kaltenegger & Sasselov 2011). The OHZ in our solar system lies between 0.75–1.8 AU, where the inner edge is the “recent Venus” limit, based on the empirical observation that the surface of Venus has been dry for at least a billion years, and the outer edge is the “early Mars” limit, based on the observation that Mars appears to have been habitable ~3.8 Gyrs ago (Kopparapu et al. 2013). The positions of the HZ boundaries vary in other planetary systems in accordance with multiple factors including the effective temperature, stellar flux and luminosity of a host star.

A primary goal of the *Kepler* mission was to determine the occurrence rate of terrestrial-size planets within the HZ of their host stars. Kane et al. (2016) cataloged all Kepler candidates that were found in their HZ, providing a list of HZ exoplanet candidates using the Kepler data release 24, Q1–Q17 data vetting process, combined with the revised stellar parameters from DR25 stellar properties table. Planets were then split into 4 groups depending on their position around their host star and their radius. Categories 1 and 2 held planets that were $< 2 R_{\oplus}$ in the CHZ and OHZ respectively and Cate-

gories 3 and 4 held planets of any radius in the CHZ and OHZ respectively. In Category 4, where candidates of any size radius are found to be in the OHZ, 76 planets of size $3 R_{\oplus}$ and above were found.

Often overshadowed by the discoveries of numerous transiting Earth-size planets in recent years (e.g. Gillon et al. 2017; Dittmann et al. 2017), Jupiter-like planets are nonetheless a critical feature of a planetary system if we are to understand the occurrence of truly Solar-system like architectures. The frequency of close-in planets, with orbits $a \leq 0.5$ AU, has been investigated in great detail thanks to the thousands of *Kepler* planets (Howard et al. 2012; Fressin et al. 2013; Burke et al. 2015). In the icy realm of Jupiter analogs, giant planets in orbits beyond the ice line ~ 3 AU, radial velocity (RV) legacy surveys remain the critical source of insight. These surveys, with time baselines exceeding 15 years, have the sensitivity to reliably detect or exclude Jupiter analogs (Wittenmyer et al. 2006; Cumming et al. 2008; Wittenmyer et al. 2011; Rowan et al. 2016). For example, an analysis of the 18-year Anglo-Australian Planet search by Wittenmyer et al. (2016) yielded a Jupiter-analog occurrence rate of $6.2^{+2.8}_{-1.6}\%$ for giant planets in orbits from 3 to 7 AU. Similar studies from the Keck Planet search (Cumming et al. 2008) and the ESO planet search programs (Zechmeister et al. 2013) have arrived at statistically identical results: in general, Jupiter-like planets in Jupiter-like orbits are present around less than 10% of solar-type stars. While these giant planets are not favored in the search for Earth-like planets, the discovery of a number of these large planets in the habitable zone of their star (Diaz et al. 2016) do indicate a potential for large rocky moons also residing in the HZ.

A moon is generally defined as a celestial body that orbits around a planet or asteroid and whose orbital barycenter is located inside the surface of the host planet or asteroid. There are currently 175 known satellites orbiting the 8 planets within the solar system, most of which are in orbit around the two largest planets in our system with Jupiter hosting 69 known moons and Saturn hosting 62 known moons¹. The diverse compositions of the satellites in the solar system give insight into their formation (Canup & Ward 2002; Heller et al. 2015). Most moons are thought to be formed from accretion within the discs of gas and dust circulating around planets in the early solar system. Through gravitational collisions between the dust, rocks and gas the debris gradually builds, bonding together to form a satellite

¹ <http://www.dtm.ciw.edu/users/sheppard/satellites/>

(Elser et al. 2011). Other satellites may have been captured by the gravitational pull of a planet if the satellite passes within the planets area of gravitational influence, or Hill radius. This capture can occur either prior to formation during the proto-planet phase, as proposed in the nebula drag theory (Holt et al. 2017; Pollack et al. 1979), or after formation of the planet, also known as dynamical capture. Moons obtained via dynamical capture could have vastly different compositions to the host planet and can explain irregular satellites such as those with high eccentricities, large inclinations, or even retrograde orbits (Holt et al. 2017; Nesvorný et al. 2003). The Giant-Collision formation theory, widely accepted as the theory of the formation of Earths Moon, proposes that during formation the large proto-planet of Earth was struck by another proto-planet approximately the size of Mars that was orbiting in close proximity. The collision caused a large debris disk to orbit the Earth and from this the material the Moon was formed (Hartmann et al. 1975; Cameron & Ward 1976). The close proximity of each proto-planet explains the similarities in the compositions of the Earth and Moon while the impact of large bodies helps explain the above average size of Earths Moon (Elser et al. 2011). The large number of moons in the solar system, particularly the large number orbiting the Jovian planets, indicate a high probability of moons orbiting giant exoplanets.

Exomoons have been explored many times in the past (e.g. Williams et al. 1997; Kipping et al. 2009; Heller 2012). Exomoon habitability particularly has been explored in great detail by Dr Rene Heller, (e.g. Heller 2012; Heller & Barnes 2013; Heller & Pudritz 2015; Zollinger et al. 2017) who proposed that an exomoon may even provide a better environment to sustain life than Earth. Exomoons have the potential to be what he calls "super-habitable" because they offer a diversity of energy sources to a potential biosphere, not just a reliance on the energy delivered by a star, like earth. The biosphere of a super-habitable exomoon could receive energy from the reflected light and emitted heat of its nearby giant planet or even from the giant planet's gravitational field through tidal forces. Thus exomoons should then expect to have a more stable, longer period in which the energy received could maintain a livable temperate surface condition for life to form and thrive in.

Another leader in the search for exomoons has been the "Hunt for Exomoons with Kepler" (HEK) team; (e.g. Kipping et al. 2012, 2013a,b, 2014, 2015). Here Kipping and others investigated the potential capability and the results of *Kepler*, focusing on the use of transit timing variations (TTV's) and transit duration vari-

ations (TDV's) to detect exomoon signatures. Though several attempts to search for companions to exoplanets through high-precision space-based photometry yielded null results, the latest HEK paper (Teachey et al. 2017) indicates the potential signature of a planetary companion, exomoon Candidate Kepler-1625b I. This exomoon is yet to be confirmed and as such caution must be exercised as the data is based on only 3 planetary transits. Still, this is the closest any exomoon hunter has come to finding the first exomoon. As we await the results of the follow up observations on this single candidate, it is clear future instruments will need greater sensitivity for the detection of exomoons to prosper. While the HEK papers focused on using the TTV/TDV methodology's to detect exomoons around all of the *Kepler* planets, our paper complements this study by determining the estimated angular separation of only those Kepler planet candidates $3R_{\oplus}$ and above that are found in the optimistic HZ of their star. We choose the lower limit of $3R_{\oplus}$ as we are interested only in those planets deemed to be gas giants that have the potential to host large satellites. While there is a general consensus that the boundary between terrestrial and gaseous planets likely lies close to $1.6R_{\oplus}$, we use $3R_{\oplus}$ as our cutoff to account for uncertainties in the stellar and planetary parameters and prevent the inclusion of potentially terrestrial planets in our list, as well as planets too small to host detectable exomoons. We use these giant planets to determine the future mission capabilities required for imaging of potential HZ exomoons. We also include RV semi-amplitude calculations for follow up observations of the HZ giant planets.

In Section 2 of this paper we explore the potential of these HZ moons, citing the vast diversity of moons within our solar system. We predict the frequency of HZ giant planets using the inverse-detection-efficiency method in Section 3. In Section 4 we present the calculations and results for the estimated planet mass, Hill radius of the planet, angular separation of the planet from the host star and of any potential exomoon from its host planet, and the RV semi-amplitude of the planet on its host star. Finally, in Section 5 we discuss the calculations and their implications for exomoons and outline proposals for observational prospects of the planets and potential moons, providing discussion of caveats and concluding remarks.

2. SCIENCE MOTIVATION

Within our solar system we observe a large variability of moons in terms of size, mass, and composition. Five icy moons of Jupiter and Saturn show strong evidence of oceans beneath their surfaces: Ganymede, Europa and

Callisto at Jupiter, and Enceladus and Titan at Saturn. From the detection of water geysers and deep oceans below the icy crust of Enceladus (Porco et al. 2006; Hsu et al. 2015) to the volcanism on Io (Morabito et al. 1979), our own solar system moons display a diversity of geological phenomena and are examples of potentially life holding worlds. Indeed Ganymede, the largest moon in our solar system, has its own magnetic field (Kivelson et al. 1996), an attribute that would increase the potential habitability of a moon due to the extra protection of the moons atmosphere from its host planet (Williams et al. 1997). And while the moons within our own HZ have shown no signs of life, namely Earth’s moon and the Martian moons of Phobos and Deimos, there is still great habitability potential for the moons of giant exoplanets residing in their HZ.

The occurrence rate of moons in the HZ is intrinsically connected to the occurrence rate of giant planets in that region. We thus consider the frequency of giant planets within the OHZ. We choose to use the wider OHZ due to warming effects any exomoon will undergo as it orbits its host planet. The giant planet will increase the effective temperature of the moon due to contributions of thermal and reflected radiation from the giant planet (Hinkel & Kane 2013). Tidal effects will also play a significant role, as seen with Io. Scharf (2006) proposed that this heating mechanism can effectively increase the outer range of the HZ for a moon as the extra mechanical heating can compensate for the lack of radiative heating provided to the moon. For the same reason this could reduce the interior edge of the HZ causing any moon with surface water to undergo the runaway green house effect earlier than a lone body otherwise would, though the outwards movement of the inner edge has been found to be significantly less than that of the outer edge and so the effective habitable zone would still be widened for any exomoon. This variation could also possibly enable giant exoplanets with eccentric orbits that lie, at times, outside the OHZ to maintain habitable conditions on any connected exomoons (Hinkel & Kane 2013).

3. FREQUENCY OF HABITABLE ZONE GIANT PLANETS

The occurrence rates of terrestrial planets in the HZ has been explored many times in the literature (e.g. Howard et al. 2012; Dressing & Charbonneau 2013, 2015; Kopparapu 2013; Petigura et al. 2013). The planet occurrence rate is defined as the number of planets per star (NPPS) given a range of planetary radius and orbital period. It is simply represented by the expression

$$NPPS = \frac{N_p}{N_*} \quad (1)$$

where N_p is the real number of planets and N_* is the number of stars in the *Kepler* survey. However, N_p is unknown due to some limitations of the mission. The first limitation is produced by the duty cycle which is the fraction of time in which a target was effectively observed (Burke et al. 2015). The requirement adopted by the Kepler mission to reliably detect a planet is to observe at least three consecutive transits (Koch et al. 2010). This requirement is difficult to achieve for low duty cycles and for planets with long orbital periods. The second limitation is the photometric efficiency, the capability of the photometer to detect a transit signal for a given noise (Signal-to-Noise ratio; SNR). For a given star it is strongly dependent on the planet size since the transit depth depends on the square of the radius ratio between the planet and the star. Thus, smaller planets are more difficult to detect than the bigger ones. Finally, the transit method is limited to orbits nearly edge-on relative to the telescope line of sight. Assuming a randomly oriented circular orbit, the probability of observing a star with radius R_* being transited by a planet with semi-major axis a is given by R_*/a .

Those survey features contribute to the underestimation of the number of detectable planets orbiting the stars of the survey. Thus, to obtain N_p , the observed number of planets N_{obs} is corrected by taking the detection efficiencies described above into account. In Section 3.1, the method used to accomplish this goal is described.

3.1. The Method

The method used in this work to compute the occurrence rate, which is commonly used in the literature ((Howard et al. 2012), (Dressing & Charbonneau 2015)), is called the inverse-detection-efficiency method (Foreman-Mackey et al. 2016). It consists of calculating the occurrence rates in a diagram of radius and period binned by a grid of cells. The diagram is binned following the recommendations of the NASA ExoPAG Study Analysis Group 13, i.e, the i -th, j -th bin is defined as the interval $[1.5^{i-2}, 1.5^{i-1})R_\oplus$ and $10x[2^{j-1}, 2^j)day$. The candidates are plotted, according to their physical parameters, and the real number of planets is then computed in each cell ($N_p^{i,j}$) by summing the observed planets ($N_{obs}^{i,j}$) in the i,j bin weighted by their inverse detection probability, as

$$N_p^{i,j} = \sum_{n=1}^{N_{obs}^{i,j}} \frac{1}{p_n} \quad (2)$$

where p_n is the detection probability of planet n . Finally, the occurrence rate is calculated by Equation (3)

as a function of orbital period and planetary radius,

$$NPPS^{i,j} = \frac{N_p^{i,j}}{N_*} \quad (3)$$

3.2. Validating Methodology

We confirm that we are able to recover accurate occurrence rates by using the method described above to first compute the occurrence rates of planets orbiting M dwarfs and comparing the results with known values found by (Dressing & Charbonneau 2015) (here after DC15). DC15 used a stellar sample of 2543 stars with effective temperatures in the range of 2661–3999 K, stellar radii between 0.10 and 0.64 R_\oplus , metallicity spanning from -2.5 to 0.56 and Kepler magnitudes between 10.07 and 16.3 (Burke et al. 2015). The sample contained 156 candidates with orbital periods extending from 0.45 to 236 days and planet radii from 0.46 to 11 R_\oplus .

The real number of planets was computed in each cell using equation (2) with p_n being the average detection probability of planet n . Then equation (3) was used to calculate the occurrence rates considering the real number of planets and the total number of stars used in the sample. We then recalculated the occurrences using the candidates from DC15 but with their disposition scores and planetary radius updated by the NASA Exoplanet Archive (Akeson et al. 2013). The disposition score is a value between 0 and 1 that indicates the confidence in the KOI disposition, a higher value indicates more confidence in its disposition. The value is calculated from a Monte Carlo technique such that the score's value is equivalent to the fraction of iterations where the Robovetter yields a disposition of "Candidate" (Akeson et al. 2013). From the 156 candidates used by DC15, 28 candidates were removed from the sample because their disposition had changed in the NASA Exoplanet Archive.

We found there is a good agreement between the results obtained in this work and those obtained by DC15 in the smaller planets domain, particularly in the range of 1.5–3.0 R_\oplus , while the occurrence rates for larger planets tended to be smaller in this work than the DC15 results. As our method validation compared the occurrence rates results obtained by two works that utilize basically the same method, data and planetary physical parameters, the discrepancies we observed may have been produced by differences in the detection probabilities used.

3.3. Stellar Sample

We selected a sample of 99,417 stars with $2400 \text{ K} \leq T_{\text{eff}} < 6000 \text{ K}$ and $\log g \geq 4.0$ from the Q1–17 Kepler Stellar Catalog in the NASA Exoplanet Archive.

From those stars, 86,383 stars have detection probabilities computed in the range of 0.6–25 R_\oplus and 5–700 days (Burke, private communication). The average detection probability was calculated for each G, K and M stars subsample and then used to compute the occurrence rates as a function of spectral type as described in Section 3.1. The number of stars in each spectral type category are shown in Table 1, where the properties of the stars in each category follow the prescription of the NASA ExoPAG Study Analysis Group 13. Figure 1 shows the diagram divided into cells which are superimposed by the average detection probability for G stars.

3.4. Planet Candidates Properties

The properties of all 4034 candidates/confirmed planets were downloaded from the Q1–17 Kepler Object of Interest on the NASA Exoplanet Archive. From this we selected 2,586 candidates that orbit the sample of stars described in the previous section and whose planetary properties lie inside the range of parameters in which the detection efficiencies were calculated. We took a conservative approach and discarded candidates with disposition scores smaller than 0.9. The properties of the resulting candidate sample range from 0.67–22.7 R_\oplus and from 5.0–470 day orbits. The planetary sample was divided into subsamples according to the spectral type of their host stars, leaving us with 1207 planets orbiting G stars, 534 planets orbiting K stars and 93 planets orbiting M stars.

3.5. Planet Occurrence Rates

For each sample of spectral type, the occurrence rates were computed for each cell spanning a range of planet radius and orbital period following the method described in Section 3.1 and using equation 2. For those cells in which no candidate was observed, we estimated an upper limit based on the uncertainty of the occurrence rate as if there was one detection in the center of the bin. Figures 2, 3 and 4 show the occurrence rates for each cell. The uncertainties were estimated using the relation

$$\delta NPPS^{i,j} = \frac{NPPS^{i,j}}{\sqrt{N_p^{i,j}}} \quad (4)$$

3.6. Frequency versus Planet Radius and Insolation

Figure 5 – 10 show the occurrence rates as a function of planet radius and orbital period. Figure 5 shows the occurrence rates for planets around G stars. Number of Planets Per Star (NPPS) is plotted against the planet radius and each line represents a band of orbital periods. The data indicates that, for G stars, planets with radii

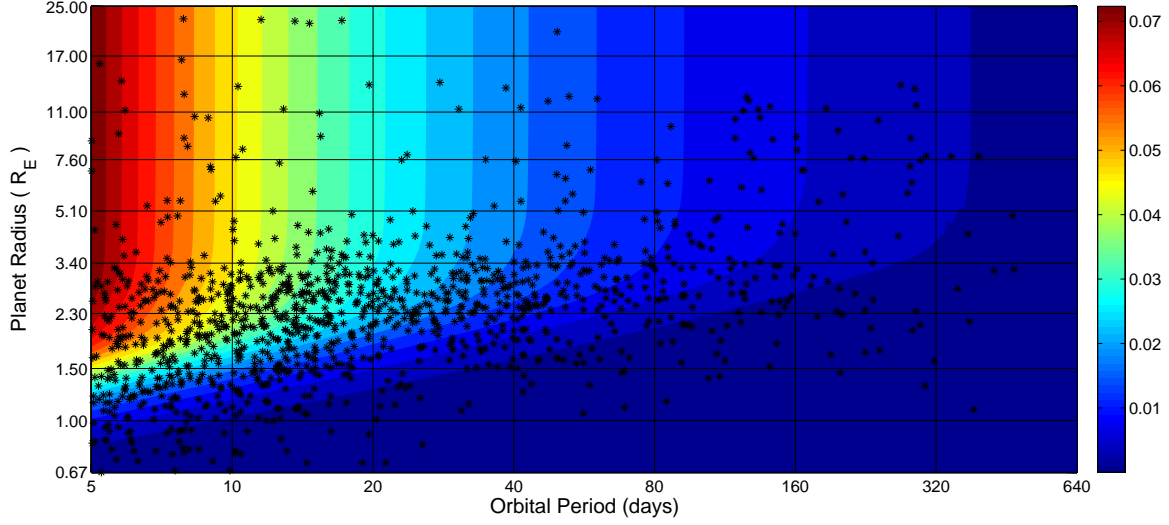


Figure 1. Average detection probability for G stars as a function of planet radius and orbital period. The star symbols represent the 1,819 *Kepler* candidates detected for these stars. Note the color bar to the right indicates the detection probability of the planets with greatest probability of detection corresponding with the top of the scale. Planets found on the top left corner of the graph will have a greater probability of detection.

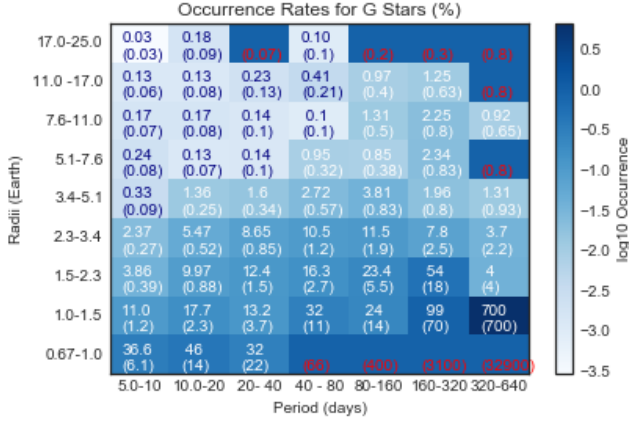


Figure 2. Binned planet occurrence rates for G stars as a function of planet radius and orbital period. Planet occurrence is given as a percentage along with uncertainty percentage (in brackets). For bins without planets we compute the uncertainty, and thus upper limit by including one detection at the center of the bin. The bins treated this way have been colored with red font for transparency.

greater than $1.5 R_{\oplus}$ are most commonly found with orbital periods between 80-320 days. The occurrence for planets with orbits between 320-640 days shows a spike for planets with radii between $1.0-1.5 R_{\oplus}$. In general, our results show that small planets are more abundant than giant planets in each orbital period bin which is consistent with Wittenmyer et al. (2011); Kane et al. (2016).

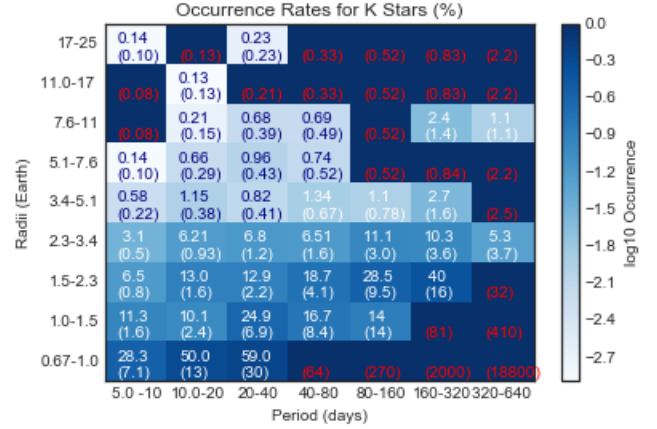


Figure 3. Binned planet occurrence rates for K stars as a function of planet radius and orbital period. Planet occurrence is given as a percentage along with uncertainty percentage (in brackets). For bins without planets we compute the uncertainty, and thus upper limit by including one detection at the center of the bin. The bins treated this way have been colored with red font for transparency.

The trends observed for K stars follows that observed for G stars; small planets are more abundant than giant planets in each orbital period bin. While Figure 8 shows a complete lack of giant planets $> 11 R_{\oplus}$ with orbital periods > 40 days, this radius range represents the rarest objects detected by *Kepler*, thus there is a lack of sufficient data to complete the calculations of their oc-

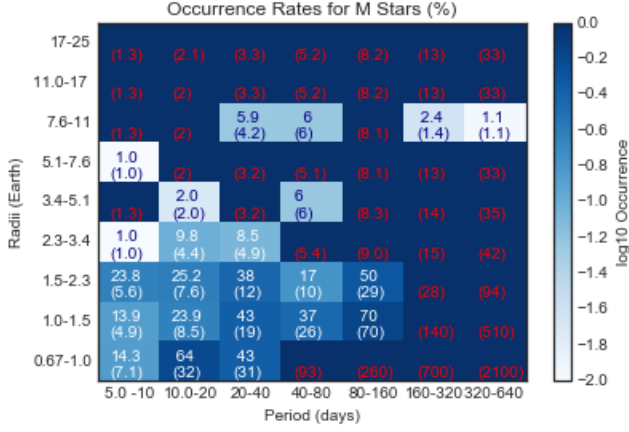


Figure 4. Binned planet occurrence rates for M stars as a function of planet radius and orbital period. Planet occurrence is given as a percentage along with uncertainty percentage (in brackets). For bins without planets we compute the uncertainty, and thus upper limit by including one detection at the center of the bin. The bins treated this way have been colored with red font for transparency.

Table 1. Planet Occurrence rates of giant planets $> 3 R_{\oplus}$ in the OHZ of their star.

Spectral Type	T_{eff} (K)	No. stars	Planets in OHZ	NPPS (%)
G	5300–6000	59510	12	6.5 ± 1.9
K	3900–5300	24560	14	11.5 ± 3.1
M	2400–3900	2313	1	6.0 ± 6.0

currence rates. In addition, there appears to be a lack of planets with radius $5.1\text{--}7.6 R_{\oplus}$ with orbits of > 80 days.

For M stars, the occurrences for different orbital periods are very similar. We observe a lack of any giant planets with $R_p > 11 R_{\oplus}$ (Figure 9). Planets with $R_p = 7.6\text{--}11 R_{\oplus}$ tend to be found with orbital periods between 20–80 days.

3.7. Frequency of Giants in the Habitable Zone

The OHZ for each host candidate was computed following the model described by Kopparapu et al. (2013, 2014). From the sample of candidates selected and described in Section 3.3, 12 candidates orbit within the OHZ of their respective G host stars, 14 candidates orbit in the OHZ of their K host stars and only 1 candidate orbits in the OHZ of an M star. The properties of the spectral type bins and the occurrence rates of giant planets in the OHZ is shown in Table 1.

4. PROPERTIES OF HABITABLE ZONE GIANT PLANETS

Here we present the calculations for the estimated planet mass, Hill radius of the planet, angular separation of the planet from the host star and of any potential exomoon from its host planet, both estimates of which can be used in deciding the ideal candidates for future imaging missions, and finally the RV semi-amplitude of the planet on its host star for use in follow up observations of each giant planet.

We start by estimating the mass of each of the Kepler candidates using the mass/radius relation found in Chen & Kipping (2016):

$$R_p = M_p^{0.59} \quad (5)$$

where R_p is the planet radius in Earth radii and M_p is planet mass in Earth masses.

As is noted in Chen & Kipping (2016), this relationship is only reliable up to $\sim 10 R_{\oplus}$. As planets $10 R_{\oplus}$ and above can vary greatly in density and thus greatly in mass, we have chosen to quantify each exoplanet with a radius of $10 R_{\oplus}$ or greater as 3 set masses; 1 Saturn mass for the very low density planets, 1 Jupiter mass for a direct comparison with our solar system body, and 13 Jupiter mass for the higher density planets. As there is discrepancy as to the mass of a planet vs brown dwarf we have chosen to use the upper limit of 13 Jupiter masses. For any planet found to have a mass larger than this the Hill radius and RV signal will thus be greater than that calculated.

Using our mass estimate, we first consider the radius at which a moon is gravitationally bound to a planet, calculating the Hill radius using Hinkel & Kane (2013):

$$r_H = a_{sp} \chi (1 - e_{sp}) \left(\frac{M_p}{M_{\star}} \right)^{\frac{1}{3}} \quad (6)$$

where M_{\star} is the mass of the host star. Assuming an eccentricity of the planet–star system of $e = 0$, the above equation becomes:

$$r_H = a_{sp} \chi \left(\frac{M_p}{M_{\star}} \right)^{\frac{1}{3}} \quad (7)$$

The factor χ is added to take into account the fact that the Hill radius is just an estimate. Other effects may impact the gravitational stability of the system, so following (Barnes & O’Brien 2002), (Kipping 2009) and (Hinkel & Kane 2013), we have chosen to use a conservative estimate of $\chi \leq 1/3$.

The expected angular separation of the exomoon from its host planet is then calculated by:

$$\alpha'' = \frac{r_H (\chi = 1/3)}{d} \quad (8)$$

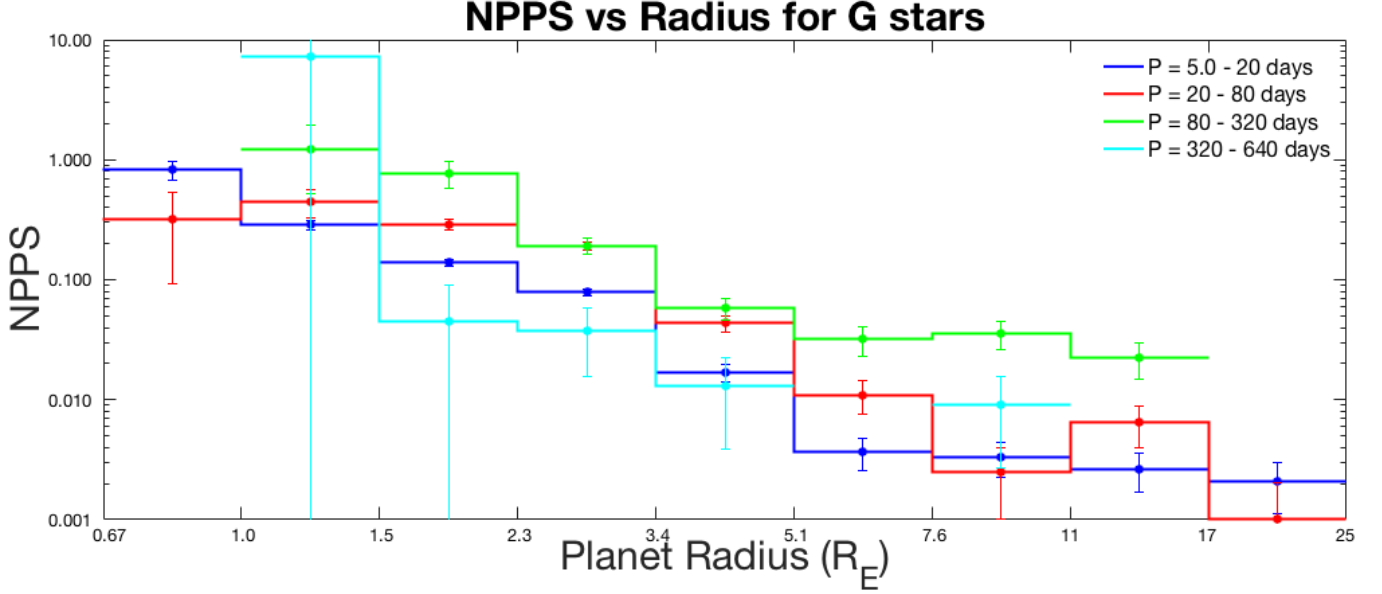


Figure 5. Number of Planets Per Star (NPPS) vs radius for G stars. Each line color represents a set range of periods. The data indicates that, for G stars, planets with radii greater than $1.5 R_{\oplus}$ are most commonly found with orbital periods between 80–320 days. Also the occurrence rate of planets with orbits between 320–640 days shows a large spike for planets with radii between 1.0–1.5 R_{\oplus} .

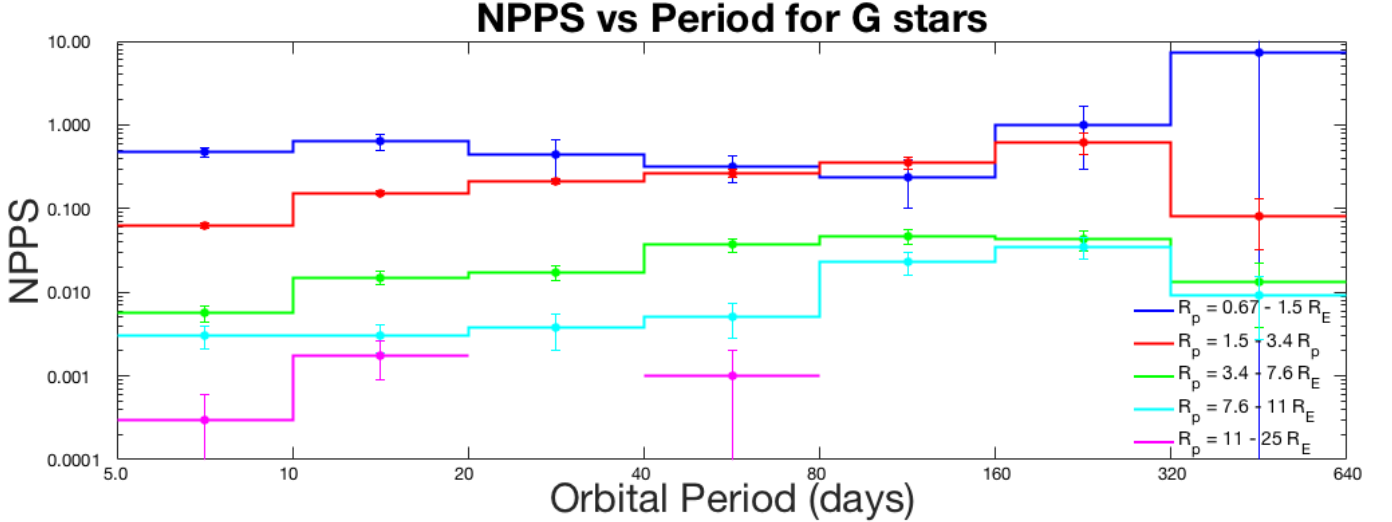


Figure 6. Number of Planets Per Star (NPPS) vs period for G stars. Each line color represents a set range of radii. The data indicates that, for G stars, small planets are more abundant than giant planets in each orbital period bin. The magenta line indicating planets with radii between 11 and 25 R_{\oplus} represents the rarest objects detected by *Kepler*, thus there is a lack of sufficient data to complete the calculations of their occurrence rates at longer orbital periods.

Here d represents the distance of the star planet system in parsecs (PC) and Hill radius is expressed in (AU).

Finally, we calculate the RV semi-amplitude, K , of each planet given its estimated mass:

$$K = \frac{(2\pi G)}{P^{1/3}} \frac{(M_p \sin i)}{((M_{\star} + M_p)^{2/3}} \quad (9)$$

We further assume an orbital inclination of $\sim 90^\circ$ and $e = 0$.

Table 2 includes each of the parameters used in our calculations which have been extracted from the HZ catalogue (Kane et al. 2016) as well as the NASA exoplanet archive. Table 3 presents our calculations of planet mass, Hill radii, estimated RV semi-amplitudes and angular separations of the planet – star systems and potential planet – moon systems at both the full Hill radii (HR) and $\frac{1}{3}$ Hill radii ($\frac{1}{3}$ HR).

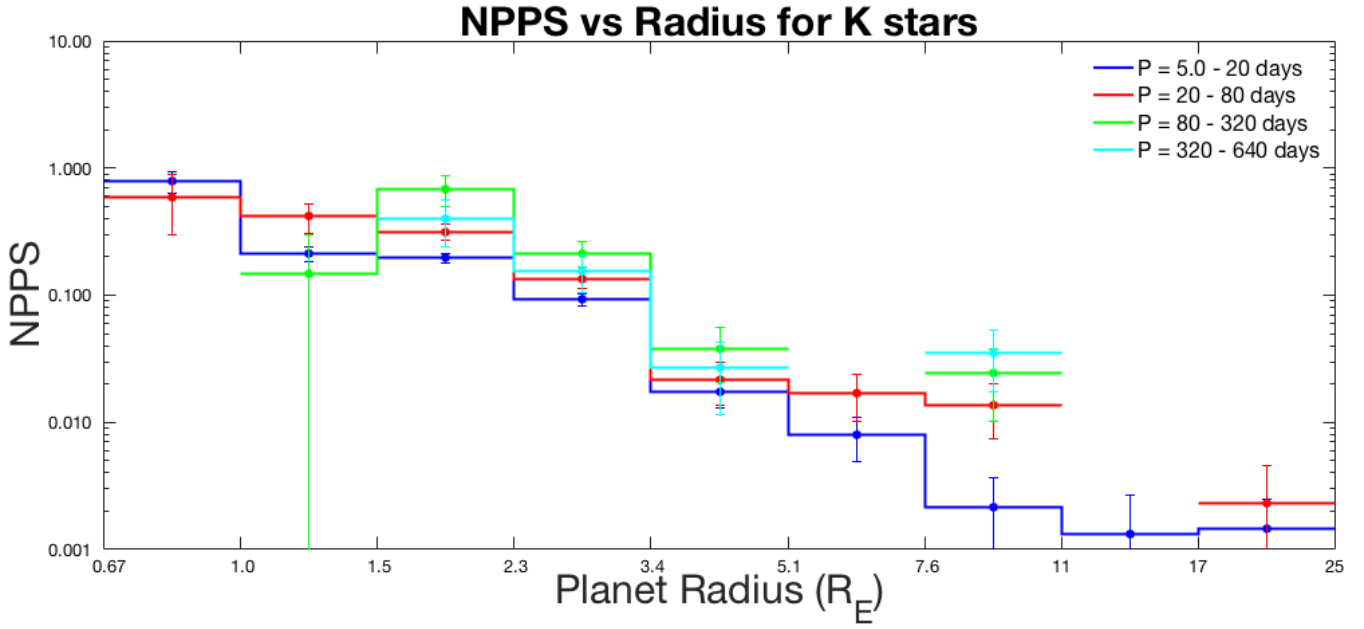


Figure 7. Number of Planets Per Star (NPPS) vs radius for K stars. Each line color represents a set range of periods. The data indicates that planets with radii between $1.5\text{--}5.1 R_{\oplus}$ most commonly have orbital periods between 80–320 days. Also, for K stars, small planets are more abundant than giant planets in each orbital period bin.

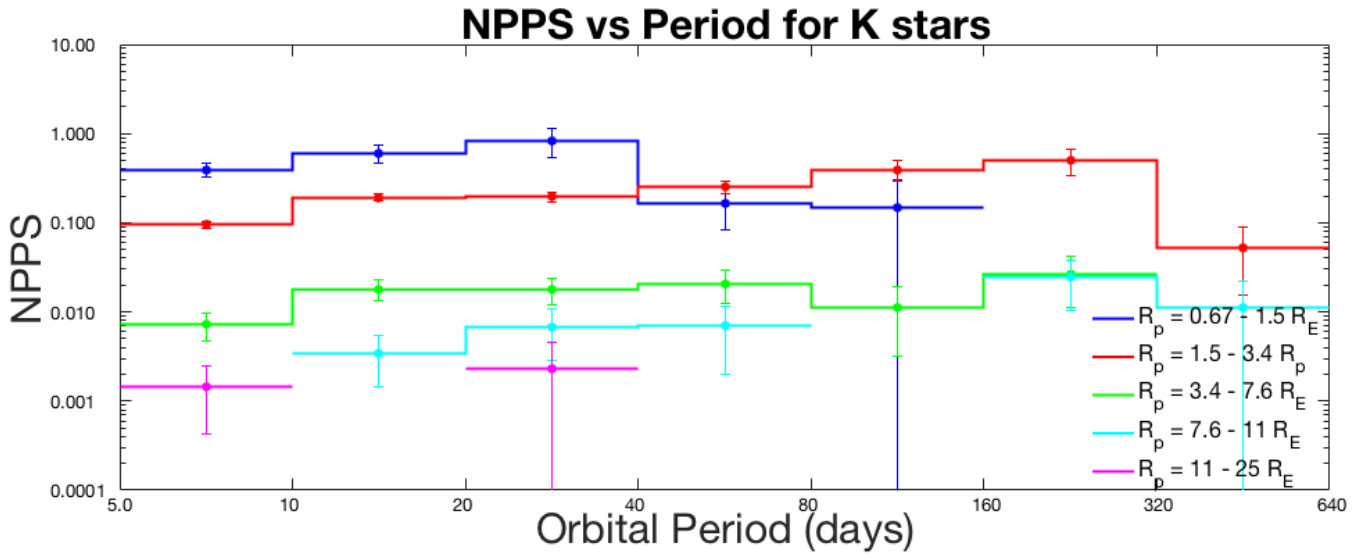


Figure 8. Number of Planets Per Star (NPPS) vs period for K stars. Each line color represents a set range of radii. Note there is a drop in the blue line representing the lowest mass planets between $0.67\text{--}1.5 R_{\oplus}$ at an orbital period of 40 days. This corresponds to the limit of detection efficiency of *Kepler* for small planets and thus there is not sufficient data in this region to claim that this is a significant drop.

Tables 4 and 5 then present our calculations of Hill radii, angular separations of a potential planet–moon systems at the full Hill radius and RV semi-amplitudes

for each exoplanet with a radius of $10R_{\oplus}$ or greater with our chosen quantified masses; 1 Saturn mass (M_{sat}), 1 Jupiter mass (M_J), and 13 Jupiter masses ($13M_J$).

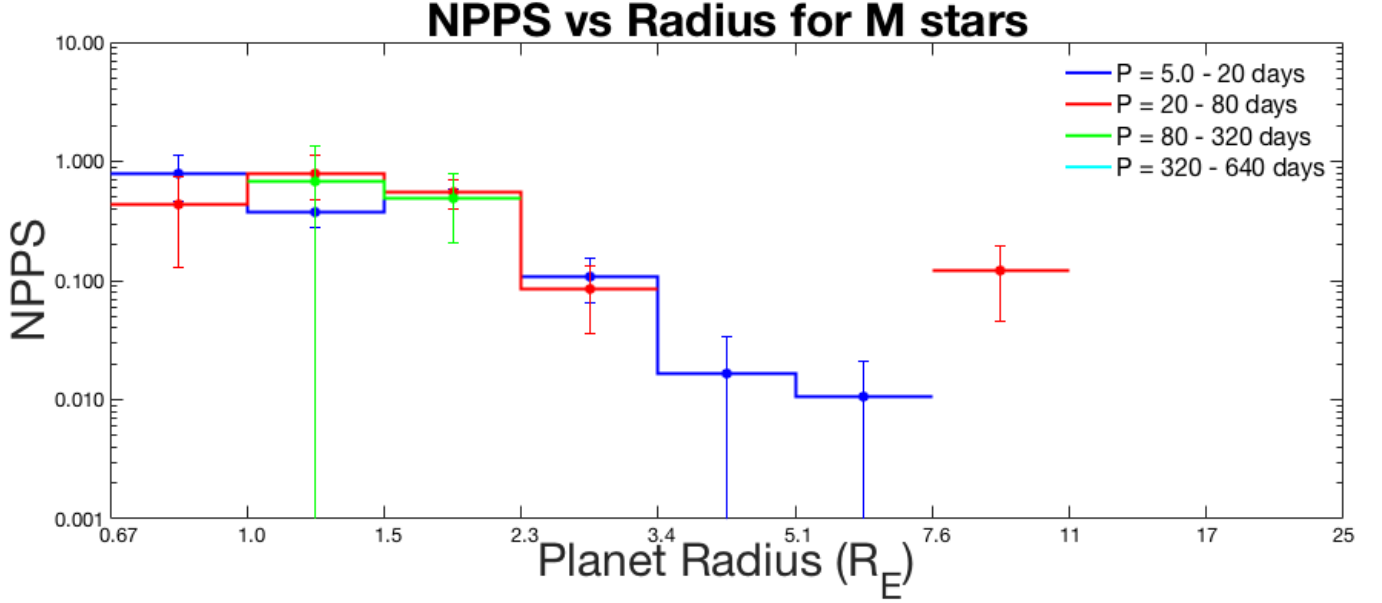


Figure 9. Number of Planets Per Star (NPPS) vs radius for M stars. Each line color represents a set range of periods. We observe a lack of any planets with $R_p > 11 R_\oplus$. Planets with $R_p = 7.6\text{--}11 R_\oplus$ tend to be found with orbital periods between 20–80 days.

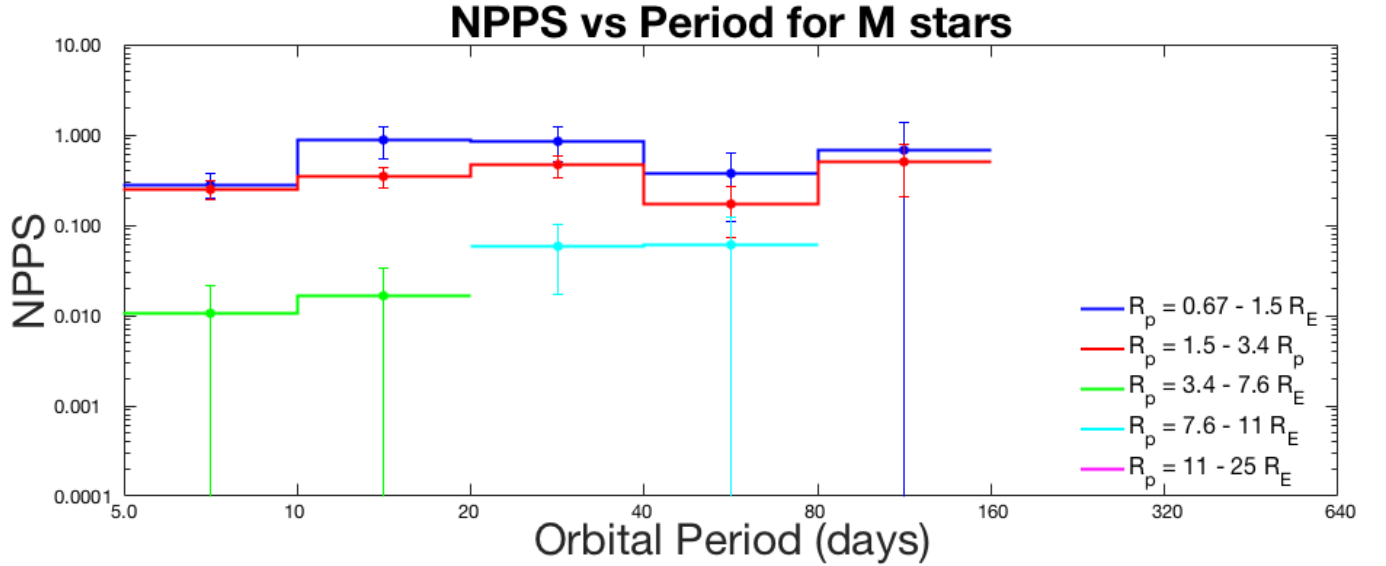


Figure 10. Number of Planets Per Star (NPPS) vs period for M stars. Each line color represents a set range of radii. We observe that small planets tend to be more abundant than giant planets in each orbital period bin. Note the drop in planets beyond an orbital period of 160 days corresponds with the limit of *Kepler* detection efficiency for these dim stars.

Table 2. Habitable Zone candidates with $R_p > 3 R_\oplus$.

KOI name	Kepler	T_{eff}	Period	a^*	Planet Radius	Incident Flux	Stellar Mass	Distance	Magnitude
		K	days	AU	R_\oplus	F_\oplus	M_\star	PC	Kepler Band
K03086.01	—	5201 ± 83	174.732 ± 0.003	0.573	3 ± 0.235	1.61 ± 0.35	0.82 ± 0.05	1006 ± 84	15.71

Table 2 continued

Table 2 (continued)

KOI name	Kepler	T_{eff}	Period	a^*	Planet Radius	Incident Flux	Stellar Mass	Distance	Magnitude
		K	days	AU	R_{\oplus}	F_{\oplus}	M_*	PC	Kepler Band
K06786.01	—	5883 ± 186	455.624 ± 0.026	1.153	3 ± 0.585	0.64 ± 0.33	0.99 ± 0.13	3192 ± 550	11.97
K02691.01	—	4735 ± 170	97.446 ± 0	0.373	3.05 ± 0.265	1.53 ± 0.49	0.73 ± 0.07	447 ± 50	14.98
K01581.02	896b	5510 ± 158	144.552 ± 0.003	0.516	3.06 ± 0.475	2 ± 0.85	0.88 ± 0.09	926 ± 170	15.48
K08156.01	—	6429 ± 182	364.982 ± 0.011	1.048	3.12 ± 0.69	1.74 ± 0.96	1.15 ± 0.16	978 ± 240	14.32
K07700.01	—	6382 ± 180	631.569 ± 0.013	1.491	3.13 ± 0.655	0.75 ± 0.4	1.1 ± 0.15	798 ± 177	14.00
K04016.01	1540b	4641 ± 79	125.413 ± 0	0.443	3.14 ± 0.125	1.19 ± 0.18	0.73 ± 0.04	293 ± 18	14.07
K05706.01	1636b	5977 ± 201	425.484 ± 0.009	1.155	3.2 ± 0.61	0.9 ± 0.46	1.13 ± 0.13	1589 ± 348	15.81
K02210.02	1143c	4895 ± 78	210.631 ± 0.002	0.648	3.23 ± 0.15	0.71 ± 0.11	0.82 ± 0.04	607 ± 38	15.20
K08276.01	—	6551 ± 183	385.859 ± 0.005	1.107	3.23 ± 0.705	1.93 ± 1.05	1.22 ± 0.17	944 ± 216	13.99
K04121.01	1554b	5275 ± 83	198.089 ± 0.002	0.631	3.24 ± 0.36	1.64 ± 0.47	0.86 ± 0.05	1164 ± 143	15.72
K05622.01	1635b	5474 ± 158	469.613 ± 0.014	1.117	3.24 ± 0.46	0.38 ± 0.15	0.85 ± 0.09	944 ± 160	15.70
K07982.01	—	6231 ± 207	376.38 ± 0.047	1.029	3.26 ± 0.665	1.17 ± 0.63	1.03 ± 0.13	1436 ± 333	15.63
K03946.01	1533b	6325 ± 79	308.544 ± 0.002	0.963	3.28 ± 0.565	2.82 ± 1.12	1.25 ± 0.11	734 ± 119	13.22
K08232.01	—	5573 ± 174	189.184 ± 0.004	0.610	3.31 ± 0.77	2.24 ± 1.32	0.85 ± 0.1	865 ± 212	15.05
K05625.01	—	5197 ± 181	116.454 ± 0.002	0.414	3.33 ± 0.375	2.07 ± 0.75	0.7 ± 0.07	894 ± 132	16.02
K02073.01	357d	5036 ± 200	49.5 ± 0	0.246	3.43 ± 2.04	6.57 ± 8.8	0.79 ± 0.04	771 ± 51	15.57
K02686.01	—	4658 ± 93	211.033 ± 0.001	0.627	3.43 ± 0.17	0.51 ± 0.09	0.74 ± 0.04	267 ± 17	13.86
K01855.01	—	4338 ± 125	58.43 ± 0	0.248	3.45 ± 0.3	1.92 ± 0.55	0.59 ± 0.06	298 ± 33	14.78
K02828.02	—	4817 ± 176	505.463 ± 0.008	1.153	3.46 ± 0.315	0.25 ± 0.08	0.8 ± 0.05	769 ± 95	15.77
K02926.05	—	3891 ± 78	75.731 ± 0.002	0.297	3.47 ± 0.19	0.74 ± 0.14	0.61 ± 0.03	425 ± 35	16.28
K08286.01	—	5440 ± 180	191.037 ± 0.013	0.634	3.54 ± 0.6	1.59 ± 0.75	0.93 ± 0.09	1654 ± 335	16.65
K01830.02	967c	5180 ± 103	198.711 ± 0.001	0.625	3.56 ± 0.215	1.06 ± 0.21	0.83 ± 0.05	502 ± 37	14.44
K00951.02	258c	4942 ± 200	33.653 ± 0	0.193	3.61 ± 2.43	12.16 ± 18.1	0.83 ± 0.05	1542 ± 431	15.22
K01986.01	1038b	5159 ± 82	148.46 ± 0.001	0.524	3.61 ± 0.205	1.56 ± 0.28	0.87 ± 0.04	606 ± 42	14.84
K01527.01	—	5401 ± 107	192.667 ± 0.001	0.622	3.64 ± 0.32	1.52 ± 0.39	0.86 ± 0.05	743 ± 71	14.88
K05790.01	—	4899 ± 82	178.267 ± 0.003	0.571	3.71 ± 0.21	0.81 ± 0.14	0.82 ± 0.04	643 ± 44	15.52
K08193.01	—	5570 ± 158	367.948 ± 0.005	0.996	3.72 ± 0.6	0.64 ± 0.28	0.97 ± 0.09	1116 ± 202	15.72
K08275.01	—	5289 ± 176	389.876 ± 0.007	1.002	3.76 ± 0.46	0.44 ± 0.17	0.89 ± 0.08	975 ± 152	15.95
K01070.02	266c	5885 ± 250	107.724 ± 0.002	0.457	3.89 ± 1.89	5.47 ± 6.24	0.95 ± 0.06	1562 ± 280	15.59
K07847.01	—	6098 ± 217	399.376 ± 0.069	1.103	3.93 ± 1.225	2.67 ± 2.04	1.12 ± 0.17	2190 ± 713	13.28
K00401.02	149d	5381 ± 100	160.018 ± 0.001	0.571	3.96 ± 0.68	2.08 ± 0.77	0.93 ± 0.05	541 ± 56	14.00
K01707.02	315c	5796 ± 108	265.469 ± 0.006	0.791	4.15 ± 0.96	1.75 ± 0.8	0.88 ± 0.06	1083 ± 147	15.32
K05581.01	1634b	5636 ± 171	374.878 ± 0.008	1.053	4.27 ± 1.125	1.5 ± 0.97	1.1 ± 0.13	1019 ± 272	14.51
K01258.03	—	5717 ± 165	148.272 ± 0.001	0.546	4.3 ± 0.75	2.52 ± 1.16	0.98 ± 0.11	1217 ± 245	15.77
K02683.01	—	5613 ± 152	126.445 ± 0	0.473	4.49 ± 0.635	2.52 ± 0.99	0.89 ± 0.1	947 ± 147	15.50
K00881.02	712c	5067 ± 102	226.89 ± 0.001	0.673	4.53 ± 0.26	0.73 ± 0.14	0.79 ± 0.04	854 ± 59	15.86
K01429.01	—	5644 ± 80	205.913 ± 0.001	0.679	4.68 ± 0.5	1.86 ± 0.5	0.98 ± 0.06	1232 ± 135	15.53
K00902.01	—	3960 ± 124	83.925 ± 0	0.303	4.78 ± 0.405	0.62 ± 0.18	0.53 ± 0.04	348 ± 43	15.75
K05929.01	—	5830 ± 158	466.003 ± 0.003	1.165	4.92 ± 0.875	0.59 ± 0.27	0.97 ± 0.12	780 ± 168	14.69
K00179.02	458b	6226 ± 118	572.377 ± 0.006	1.406	5.8 ± 0.905	1.15 ± 0.45	1.13 ± 0.09	904 ± 140	13.96
K03823.01	—	5536 ± 79	202.117 ± 0.001	0.667	5.8 ± 0.53	1.59 ± 0.38	0.96 ± 0.05	563 ± 57	13.92
K01058.01	—	3337 ± 86	5.67 ± 0	0.034	5.85 ± 2.015	3.22 ± 2.55	0.16 ± 0.07	32 ± 12	13.78
K00683.01	—	5799 ± 110	278.124 ± 0	0.842	5.86 ± 0.72	1.58 ± 0.51	1.03 ± 0.07	622 ± 73	13.71
K05375.01	—	5142 ± 150	285.375 ± 0.004	0.794	5.94 ± 4.05	7.56 ± 11.19	0.82 ± 0.21	1138 ± 769	13.86
K05833.01	—	6261 ± 174	440.171 ± 0.006	1.145	5.97 ± 1.53	2.97 ± 1.85	1.03 ± 0.16	809 ± 200	13.01
K02076.02	1085b	6063 ± 181	219.322 ± 0.001	0.739	6.11 ± 1.085	2.27 ± 1.08	1.12 ± 0.14	1314 ± 270	15.27
K02681.01	397c	5307 ± 100	135.499 ± 0.001	0.480	6.18 ± 0.56	1.83 ± 0.47	0.78 ± 0.05	983 ± 76	16.00
K05416.01	1628b	3869 ± 140	76.378 ± 0.002	0.295	6.28 ± 0.6	0.79 ± 0.26	0.59 ± 0.06	418 ± 56	16.60

Table 2 continued

Table 2 (*continued*)

KOI name	Kepler	T_{eff}	Period	a^*	Planet Radius	Incident Flux	Stellar Mass	Distance	Magnitude
		K	days	AU	R_{\oplus}	F_{\oplus}	M_{\star}	PC	Kepler Band
K01783.02	—	5791 ± 111	284.063 ± 0.002	0.845	6.36 ± 1.105	2.52 ± 1.07	1 ± 0.08	913 ± 157	13.93
K02689.01	—	5594 ± 186	165.345 ± 0	0.547	6.98 ± 1.175	1.94 ± 0.91	0.8 ± 0.08	1001 ± 191	15.55
K05278.01	—	5330 ± 187	281.592 ± 0.001	0.776	7.22 ± 0.885	0.61 ± 0.24	0.8 ± 0.08	911 ± 133	15.87
K03791.01	460b	6340 ± 190	440.784 ± 0.001	1.146	7.23 ± 2	2.14 ± 1.44	1.03 ± 0.15	917 ± 242	13.77
K01375.01	—	6018 ± 120	321.212 ± 0	0.945	7.25 ± 1.165	2.18 ± 0.87	1.09 ± 0.09	755 ± 129	13.71
K03263.01	—	3638 ± 76	76.879 ± 0	0.275	7.71 ± 0.83	0.4 ± 0.12	0.47 ± 0.05	220 ± 28	15.95
K01431.01	—	5597 ± 112	345.159 ± 0	0.975	7.79 ± 0.745	0.8 ± 0.22	1.03 ± 0.06	456 ± 48	13.46
K01439.01	849b	5910 ± 113	394.625 ± 0.001	1.109	7.79 ± 1.585	2.66 ± 1.28	1.16 ± 0.13	740 ± 147	12.85
K01411.01	—	5716 ± 109	305.076 ± 0	0.912	7.82 ± 1.045	1.54 ± 0.53	1.08 ± 0.07	537 ± 75	13.38
K00950.01	—	3748 ± 59	31.202 ± 0	0.150	8.31 ± 0.575	1.59 ± 0.32	0.46 ± 0.03	237 ± 21	15.80
K05071.01	—	6032 ± 211	180.412 ± 0.001	0.637	8.86 ± 1.73	2.78 ± 1.47	1.06 ± 0.14	1373 ± 301	15.66
K03663.01	86b	5725 ± 108	282.525 ± 0	0.836	8.98 ± 0.89	1.15 ± 0.31	0.97 ± 0.06	328 ± 35	12.62
K00620.03	51c	6018 ± 107	85.312 ± 0.003	0.384	9 ± 2.25	7.05 ± 8	1.05 ± 0.14	927 ± 205	14.67
K01477.01	—	5270 ± 79	169.498 ± 0.001	0.575	9.06 ± 0.59	1.29 ± 0.24	0.9 ± 0.05	1053 ± 78	15.92
K03678.01	1513b	5650 ± 186	160.885 ± 0	0.542	9.09 ± 2.53	3.4 ± 2.34	0.82 ± 0.09	410 ± 112	12.89
K08007.01	—	3391 ± 42	67.177 ± 0	0.218	9.66 ± 1.115	0.24 ± 0.07	0.3 ± 0.04	135 ± 18	16.06
K00620.02	51d	6018 ± 107	130.194 ± 0.004	0.509	9.7 ± 0.5	4.01 ± 4.56	1.05 ± 0.14	927 ± 205	14.67
K01681.04	—	3638 ± 80	21.914 ± 0	0.117	10.39 ± 1.26	2.01 ± 0.66	0.45 ± 0.05	203 ± 30	15.86
K00868.01	—	4245 ± 85	235.999 ± 0	0.653	10.59 ± 0.435	0.29 ± 0.05	0.67 ± 0.03	358 ± 22	15.17
K01466.01	—	4810 ± 76	281.563 ± 0	0.766	10.83 ± 0.535	0.49 ± 0.08	0.76 ± 0.04	855 ± 55	15.96
K00351.01	90h	5970 ± 119	331.597 ± 0	0.965	10.89 ± 1.61	1.76 ± 0.66	1.09 ± 0.08	809 ± 118	13.80
K00433.02	553c	5234 ± 103	328.24 ± 0	0.908	10.99 ± 0.77	0.6 ± 0.13	0.93 ± 0.05	706 ± 46	14.92
K05329.01	—	6108 ± 211	200.235 ± 0.001	0.686	10.99 ± 2.305	2.64 ± 1.47	1.07 ± 0.15	1207 ± 269	15.39
K03811.01	—	5631 ± 76	290.14 ± 0	0.843	11.58 ± 2.045	2.02 ± 0.82	0.95 ± 0.06	738 ± 130	13.91
K03801.01	—	5672 ± 76	288.313 ± 0.001	0.846	13.21 ± 2.185	1.93 ± 0.74	0.97 ± 0.07	1837 ± 318	16.00
K01268.01	—	5798 ± 78	268.941 ± 0.001	0.827	13.57 ± 2.305	2.53 ± 1	1.04 ± 0.08	1262 ± 219	14.81

* Semi major axis

Table 3. Radial Velocity, Hill Radius & Angular Separation Calculations for HZ Candidates with $R_p > 3 R_{\oplus}$.

KOI name	Kepler	Planet Mass	Hill Radius	$\alpha'' \text{ Planet} - \text{Star}$	$\alpha'' \text{ Moon}(HR)$	$\alpha'' \text{ Moon}(\frac{1}{3}HR)$	Radial Velocity
		M_{\oplus}	AU	$\mu \text{ arcsec}$	$\mu \text{ arcsec}$	$\mu \text{ arcsec}$	m/s
K03086.01	—	6.44 ± 0.98	0.0114 ± 0.0006	570 ± 48	11.3 ± 1.1	3.78 ± 0.37	0.84 ± 0.15
K06786.01	—	6.44 ± 2.44	0.0216 ± 0.0029	361 ± 62	6.77 ± 1.5	2.26 ± 0.49	0.54 ± 0.23
K02691.01	—	6.62 ± 1.12	0.0078 ± 0.0005	834 ± 93	17.4 ± 2.3	5.81 ± 0.75	1.13 ± 0.24
K01581.02	896b	6.66 ± 2.01	0.0102 ± 0.0011	558 ± 102	11 ± 2.4	3.67 ± 0.78	0.89 ± 0.29
K08156.01	—	6.88 ± 2.96	0.019 ± 0.0029	1070 ± 263	19.4 ± 5.6	6.44 ± 1.86	0.56 ± 0.27
K07700.01	—	6.92 ± 2.82	0.0275 ± 0.0039	1870 ± 414	34.5 ± 9.1	11.5 ± 3.03	0.48 ± 0.22
K04016.01	1540b	6.95 ± 0.54	0.0094 ± 0.0003	1510 ± 93	32 ± 2.2	10.6 ± 0.73	1.09 ± 0.11
K05706.01	1636b	7.18 ± 2.67	0.0214 ± 0.0028	727 ± 159	13.5 ± 3.4	4.47 ± 1.14	0.56 ± 0.23
K02210.02	1143c	7.3 ± 0.66	0.0134 ± 0.0005	1070 ± 67	22.1 ± 1.6	7.42 ± 0.54	0.9 ± 0.1
K08276.01	—	7.3 ± 3.1	0.0201 ± 0.003	1170 ± 268	21.3 ± 5.8	7.1 ± 1.94	0.56 ± 0.26
K04121.01	1554b	7.33 ± 1.59	0.0129 ± 0.001	543 ± 67	11.1 ± 1.6	3.69 ± 0.54	0.89 ± 0.2
K05622.01	1635b	7.33 ± 2.03	0.0229 ± 0.0023	1180 ± 201	24.3 ± 4.8	8.05 ± 1.59	0.67 ± 0.21
K07982.01	—	7.41 ± 2.94	0.0199 ± 0.0028	716 ± 166	13.9 ± 3.8	4.6 ± 1.25	0.65 ± 0.28
K03946.01	1533b	7.49 ± 2.51	0.0175 ± 0.002	1310 ± 212	23.8 ± 4.7	7.9 ± 1.57	0.61 ± 0.22
K08232.01	—	7.6 ± 3.45	0.0127 ± 0.002	706 ± 173	14.7 ± 4.3	4.86 ± 1.41	0.95 ± 0.46
K05625.01	—	7.68 ± 1.69	0.0092 ± 0.0007	463 ± 69	10.3 ± 1.7	3.47 ± 0.58	1.28 ± 0.34

Table 3 continued

Table 3 (continued)

KOI name	Kepler	Planet Mass	Hill Radius	α'' Planet – Star	α'' Moon(HR)	α'' Moon($\frac{1}{3}$ HR)	Radial Velocity
		M_{\oplus}	AU	μ arcsec	μ arcsec	μ arcsec	m/s
K02073.01	357d	8.08 \pm 9.36	0.0053 \pm 0.0021	319 \pm 21	6.87 \pm 2.8	2.33 \pm 0.94	1.64 \pm 1.91
K02686.01	—	8.08 \pm 0.78	0.0139 \pm 0.0005	2350 \pm 150	52.1 \pm 3.8	17.2 \pm 1.26	1.06 \pm 0.13
K01855.01	—	8.16 \pm 1.38	0.0059 \pm 0.0004	832 \pm 92	19.8 \pm 2.6	6.71 \pm 0.87	1.9 \pm 0.41
K02828.02	—	8.2 \pm 1.45	0.025 \pm 0.0016	1500 \pm 185	32.5 \pm 4.5	10.8 \pm 1.5	0.76 \pm 0.15
K02926.05	—	8.24 \pm 0.88	0.0071 \pm 0.0003	698 \pm 58	16.7 \pm 1.6	5.65 \pm 0.52	1.74 \pm 0.22
K08286.01	—	8.52 \pm 2.81	0.0133 \pm 0.0015	383 \pm 78	8.04 \pm 1.9	2.66 \pm 0.62	0.99 \pm 0.35
K01830.02	967c	8.6 \pm 1.01	0.0137 \pm 0.0006	1250 \pm 92	27.3 \pm 2.3	9.17 \pm 0.79	1.07 \pm 0.15
K00951.02	258c	8.81 \pm 11.55	0.0042 \pm 0.0019	125 \pm 35	2.72 \pm 1.5	0.91 \pm 0.48	1.98 \pm 2.6
K01986.01	1038b	8.81 \pm 0.97	0.0113 \pm 0.0005	864 \pm 60	18.6 \pm 1.5	6.27 \pm 0.52	1.17 \pm 0.15
K01527.01	—	8.93 \pm 1.53	0.0136 \pm 0.0008	837 \pm 80	18.3 \pm 2.1	6.06 \pm 0.68	1.09 \pm 0.21
K05790.01	—	9.23 \pm 1.02	0.0128 \pm 0.0005	888 \pm 61	19.9 \pm 1.6	6.69 \pm 0.53	1.2 \pm 0.16
K08193.01	—	9.27 \pm 2.91	0.0211 \pm 0.0023	892 \pm 162	18.9 \pm 4	6.27 \pm 1.33	0.84 \pm 0.29
K08275.01	—	9.44 \pm 2.25	0.0221 \pm 0.0019	1030 \pm 160	22.7 \pm 4	7.59 \pm 1.35	0.9 \pm 0.24
K01070.02	266c	10 \pm 9.46	0.01 \pm 0.0032	293 \pm 53	6.4 \pm 2.4	2.11 \pm 0.78	1.39 \pm 1.32
K07847.01	—	10.17 \pm 6.18	0.023 \pm 0.0048	503 \pm 164	10.5 \pm 4.1	3.52 \pm 1.36	0.82 \pm 0.53
K00401.02	149d	10.3 \pm 3.45	0.0127 \pm 0.0014	1060 \pm 109	23.5 \pm 3.6	7.76 \pm 1.17	1.27 \pm 0.43
K01707.02	315c	11.16 \pm 5.03	0.0185 \pm 0.0028	731 \pm 99	17.1 \pm 3.5	5.73 \pm 1.16	1.21 \pm 0.56
K05581.01	1634b	11.71 \pm 6.01	0.0231 \pm 0.0041	1030 \pm 276	22.7 \pm 7.3	7.55 \pm 2.42	0.97 \pm 0.52
K01258.03	—	11.85 \pm 4.03	0.0125 \pm 0.0015	448 \pm 90	10.3 \pm 2.4	3.45 \pm 0.81	1.45 \pm 0.54
K02683.01	—	12.75 \pm 3.51	0.0115 \pm 0.0011	499 \pm 78	12.1 \pm 2.2	4.01 \pm 0.73	1.76 \pm 0.55
K00881.02	712c	12.94 \pm 1.45	0.0171 \pm 0.0007	788 \pm 55	20 \pm 1.6	6.67 \pm 0.54	1.59 \pm 0.22
K01429.01	—	13.68 \pm 2.85	0.0163 \pm 0.0012	551 \pm 60	13.2 \pm 1.8	4.38 \pm 0.58	1.5 \pm 0.34
K00902.01	—	14.18 \pm 2.34	0.0091 \pm 0.0006	872 \pm 108	26.2 \pm 3.7	8.63 \pm 1.21	3.18 \pm 0.63
K05929.01	—	14.89 \pm 5.16	0.029 \pm 0.0035	1490 \pm 322	37.2 \pm 9.2	12.4 \pm 3.07	1.25 \pm 0.48
K00179.02	458b	19.68 \pm 5.98	0.0365 \pm 0.0038	1560 \pm 241	40.4 \pm 7.5	13.5 \pm 2.52	1.4 \pm 0.45
K03823.01	—	19.68 \pm 3.5	0.0182 \pm 0.0011	1180 \pm 120	32.3 \pm 3.8	10.8 \pm 1.28	2.2 \pm 0.43
K01058.01	—	19.96 \pm 13.39	0.0017 \pm 0.0004	1070 \pm 407	53.7 \pm 23.9	18.9 \pm 8.45	23.89 \pm 21.28
K00683.01	—	20.02 \pm 4.79	0.0227 \pm 0.0019	1350 \pm 159	36.5 \pm 5.3	12.2 \pm 1.76	1.92 \pm 0.5
K05375.01	—	20.49 \pm 27.21	0.0232 \pm 0.0105	697 \pm 471	20.4 \pm 16.6	6.76 \pm 5.5	2.28 \pm 3.14
K05833.01	—	20.66 \pm 10.32	0.0311 \pm 0.0054	1420 \pm 350	38.4 \pm 11.6	12.9 \pm 3.88	1.7 \pm 0.93
K02076.02	1085b	21.49 \pm 7.43	0.0198 \pm 0.0024	562 \pm 116	15.1 \pm 3.6	5.02 \pm 1.2	2.12 \pm 0.82
K02681.01	397c	21.91 \pm 3.87	0.0146 \pm 0.0009	488 \pm 38	14.8 \pm 1.5	4.98 \pm 0.49	3.21 \pm 0.63
K05416.01	1628b	22.51 \pm 4.19	0.01 \pm 0.0007	706 \pm 95	23.9 \pm 3.6	7.89 \pm 1.19	4.84 \pm 1.11
K01783.02	—	23 \pm 7.78	0.0241 \pm 0.0028	925 \pm 159	26.4 \pm 5.5	8.76 \pm 1.82	2.24 \pm 0.8
K02689.01	—	26.93 \pm 8.83	0.0177 \pm 0.002	546 \pm 104	17.7 \pm 3.9	5.89 \pm 1.31	3.65 \pm 1.31
K05278.01	—	28.52 \pm 6.81	0.0256 \pm 0.0022	852 \pm 124	28.1 \pm 4.8	9.33 \pm 1.58	3.24 \pm 0.91
K03791.01	460b	28.59 \pm 15.4	0.0347 \pm 0.0064	1250 \pm 329	37.8 \pm 12.2	12.6 \pm 4.07	2.35 \pm 1.36
K01375.01	—	28.72 \pm 8.99	0.0281 \pm 0.003	1250 \pm 214	37.2 \pm 7.5	12.4 \pm 2.51	2.53 \pm 0.85
K03263.01	—	31.88 \pm 6.68	0.0112 \pm 0.0009	1250 \pm 159	50.8 \pm 7.7	16.8 \pm 2.53	7.96 \pm 2.02
K01431.01	—	32.44 \pm 6.04	0.0308 \pm 0.002	2140 \pm 225	67.6 \pm 8.4	22.6 \pm 2.8	2.9 \pm 0.58
K01439.01	849b	32.44 \pm 12.86	0.0336 \pm 0.0046	1500 \pm 298	45.4 \pm 11	15.1 \pm 3.66	2.56 \pm 1.09
K01411.01	—	32.65 \pm 8.5	0.0284 \pm 0.0025	1700 \pm 237	52.9 \pm 8.7	17.7 \pm 2.92	2.94 \pm 0.81
K00950.01	—	36.19 \pm 4.88	0.0064 \pm 0.0003	633 \pm 56	27 \pm 2.7	8.87 \pm 0.89	12.32 \pm 2.01
K05071.01	—	40.35 \pm 15.35	0.0215 \pm 0.0029	464 \pm 102	15.7 \pm 4	5.25 \pm 1.35	4.41 \pm 1.87
K03663.01	86b	41.28 \pm 7.97	0.0292 \pm 0.002	2550 \pm 272	89 \pm 11.3	29.6 \pm 3.75	4.09 \pm 0.88
K00620.03	51c	41.43 \pm 20.18	0.0131 \pm 0.0022	414 \pm 92	14.1 \pm 3.9	4.75 \pm 1.32	5.81 \pm 3.02
K01477.01	—	41.9 \pm 5.32	0.0207 \pm 0.0009	546 \pm 41	19.7 \pm 1.7	6.55 \pm 0.56	5.19 \pm 0.76
K03678.01	1513b	42.14 \pm 22.84	0.0202 \pm 0.0037	1320 \pm 361	49.3 \pm 16.2	16.3 \pm 5.38	5.66 \pm 3.2
K08007.01	—	46.71 \pm 10.5	0.0117 \pm 0.001	1610 \pm 214	86.5 \pm 13.7	28.8 \pm 4.56	16.25 \pm 4.89
K00620.02	51d	47.04 \pm 4.72	0.0181 \pm 0.001	549 \pm 121	19.5 \pm 4.5	6.47 \pm 1.48	5.73 \pm 1.19
K01681.04	—	52.85 \pm 12.48	0.0058 \pm 0.0005	578 \pm 87	28.6 \pm 4.9	9.36 \pm 1.62	20.56 \pm 5.87
K00868.01	—	54.59 \pm 4.37	0.0284 \pm 0.0009	1830 \pm 112	79.4 \pm 5.5	26.6 \pm 1.84	7.41 \pm 0.77
K01466.01	—	56.7 \pm 5.46	0.0323 \pm 0.0012	896 \pm 58	37.8 \pm 2.8	12.6 \pm 0.94	6.67 \pm 0.78
K00351.01	90h	57.23 \pm 16.48	0.0362 \pm 0.0036	1190 \pm 174	44.8 \pm 7.9	15 \pm 2.64	4.99 \pm 1.54
K00433.02	553c	58.13 \pm 7.93	0.0361 \pm 0.0017	1290 \pm 84	51.2 \pm 4.1	17 \pm 1.37	5.67 \pm 0.87
K05329.01	—	58.13 \pm 23.75	0.026 \pm 0.0037	568 \pm 127	21.5 \pm 5.7	7.21 \pm 1.91	6.06 \pm 2.74
K03811.01	—	63.52 \pm 21.85	0.0343 \pm 0.004	1140 \pm 201	46.4 \pm 9.8	15.4 \pm 3.26	6.36 \pm 2.27
K03801.01	—	79.4 \pm 25.58	0.0368 \pm 0.004	461 \pm 80	20 \pm 4.1	6.7 \pm 1.37	7.85 \pm 2.65
K01268.01	—	83.1 \pm 27.5	0.0356 \pm 0.004	655 \pm 114	28.2 \pm 5.8	9.43 \pm 1.95	8.01 \pm 2.77

We plot a histogram of the effective temperatures of Kepler host stars to determine if there is a similar distri-

bution of temperatures among both the HZ candidates and the full catalog.

Table 4. Radial Velocity Semi-amplitude calculations for Category 4 HZ candidates with $R_p > 10 R_\oplus$.

KOI name	Kepler	Period	Planet Radius	Stellar Mass	RV (M_{sat})	RV (M_J)	RV ($13M_J$)
		Days	R_\oplus	M_\star	m/s	m/s	m/s
K01681.04		21.914 ± 0.0002	10.39 ± 1.26	0.45 ± 0.051	37.03 ± 5.94	123.73 ± 20.08	1621.95 ± 258.66
K00868.01		235.999 ± 0.0003	10.59 ± 0.435	0.666 ± 0.031	12.91 ± 0.86	43.13 ± 3.06	563.9 ± 38.53
K01466.01		281.563 ± 0.0004	10.83 ± 0.535	0.755 ± 0.036	11.2 ± 0.76	37.4 ± 2.71	488.67 ± 34.16
K00351.01	90h	331.597 ± 0.0003	10.89 ± 1.61	1.089 ± 0.084	8.3 ± 0.91	27.74 ± 3.11	361.88 ± 39.94
K00433.02	553c	328.24 ± 0.0004	10.99 ± 0.77	0.927 ± 0.045	9.28 ± 0.64	30.99 ± 2.28	404.54 ± 28.79
K05329.01		200.235 ± 0.0006	10.99 ± 2.305	1.072 ± 0.146	9.93 ± 1.91	33.17 ± 6.45	432.68 ± 83.35
K03811.01		290.14 ± 0.0003	11.58 ± 2.045	0.947 ± 0.064	9.53 ± 0.91	31.84 ± 3.16	415.53 ± 40.36
K03801.01		288.313 ± 0.0005	13.21 ± 2.185	0.969 ± 0.068	9.41 ± 0.94	31.42 ± 3.23	410.03 ± 41.29
K01268.01		268.941 ± 0.0005	13.57 ± 2.305	1.041 ± 0.075	9.18 ± 0.94	30.65 ± 3.23	399.95 ± 41.32

Table 5. Hill Radii calculations for Category 4 HZ candidates with $R_p > 10 R_\oplus$.

KOI name	Kepler	Planet Radius	Hill Radius (M_{sat})	Hill Radius (M_J)	Hill Radius ($13 M_J$)	α'' (M_{sat}) ^a	α'' (M_J) ^b	α'' ($13M_J$) ^c
		R_\oplus	AU	AU	AU	μ arcsec	μ arcsec	μ arcsec
K01681.04		10.39 ± 1.26	0.007 ± 0.0003	0.0105 ± 0.0004	0.0246 ± 0.0009	28.6 ± 4.9	9.4 ± 1.6	578 ± 87
K00868.01		10.59 ± 0.435	0.0342 ± 0.0005	0.0511 ± 0.0009	0.1201 ± 0.002	79.4 ± 5.5	26.6 ± 1.8	1830 ± 112
K01466.01		10.83 ± 0.535	0.0384 ± 0.0006	0.0574 ± 0.001	0.135 ± 0.0023	37.8 ± 2.8	12.6 ± 0.9	896 ± 58
K00351.01	90h	10.89 ± 1.61	0.0429 ± 0.0011	0.0641 ± 0.0017	0.1506 ± 0.004	44.8 ± 7.9	15 ± 2.6	1190 ± 174
K00433.02	553c	10.99 ± 0.77	0.0425 ± 0.0007	0.0636 ± 0.0012	0.1495 ± 0.0026	51.2 ± 4.1	17 ± 1.4	1290 ± 84
K05329.01		10.99 ± 2.305	0.0306 ± 0.0014	0.0458 ± 0.0021	0.1076 ± 0.0049	21.5 ± 5.7	7.2 ± 1.9	568 ± 127
K03811.01		11.58 ± 2.045	0.0392 ± 0.0009	0.0586 ± 0.0014	0.1378 ± 0.0032	46.4 ± 9.8	15.4 ± 3.3	1140 ± 201
K03801.01		13.21 ± 2.185	0.039 ± 0.0009	0.0584 ± 0.0015	0.1372 ± 0.0033	20 ± 4.1	6.7 ± 1.4	461 ± 80
K01268.01		13.57 ± 2.305	0.0373 ± 0.0009	0.0557 ± 0.0014	0.131 ± 0.0033	28.2 ± 5.8	9.4 ± 2	655 ± 114

^a Angular separation of exomoon at full Hill radius for $M_p = M_{sat}$.^b Angular separation of exomoon at full Hill radius for $M_p = M_J$.^c Angular separation of exomoon at full Hill radius for $M_p = 13M_J$.

Figure 11 shows the stellar temperature distributions for both the HZ Kepler candidates (green) as well as the full Kepler catalog (gray). The histograms show that there is a similar distribution of temperatures among both the HZ candidates and the full catalog, with the HZ host star temperatures dropping off (around) 7000K. As the habitable zone of stars with greater effective temperatures will lie further away from the star, planets in this zone are harder to detect. Thus this drop is likely a false upper limit.

Using the calculations from our Tables above, we plot the Kepler magnitude of the host star of both the unconfirmed and confirmed HZ planets and their expected radial velocity signatures to determine the expected detectability of these planets.

Figure 12 shows the Kepler magnitude of the host star of both the unconfirmed and confirmed HZ planets and their expected radial velocity signatures.

We then provide a similar plot in Figure 13, this time plotting the Kepler magnitude of the host star of both the unconfirmed and confirmed HZ planets and their expected angular separations of a moon at the full Hill radius of the host planet.

Figure 14 shows the distribution of the estimated planet - moon angular separation at the full Hill radii of the candidate. It can be seen that the resolution required to image a moon is between 1 - 90 μ arcseconds with the moon positioned at its maximum stable distance from the planet. If a potential moon resides within $\frac{1}{3}$ Hill radius from the planet as expected, the resolution will need to improve as much again. Note these graphs do not take into account the separate calculations of angular separation for those planets $\geq 10R_\oplus$.

Figure 15 shows the distribution of the Hill radii of Kepler habitable zone planets $> 3R_\oplus$. Potential moons of giant planets found in the habitable zone will likely have

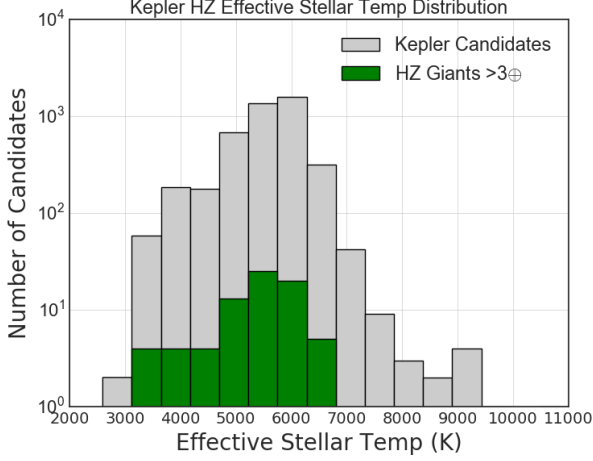


Figure 11. Stellar temperature distributions. Habitable zone Kepler candidates in green overlays the distribution of the full Kepler catalog in gray. The histograms show that there is a similar distribution of temperatures among both the HZ candidates and the full Kepler catalog. While the distribution of the habitable zone candidates drops off at 7000K, this could be a false upper limit as the habitable zone of stars with greater effective temperature lies further away from the star and current transit detection methods are less sensitive to planets at these longer orbits.

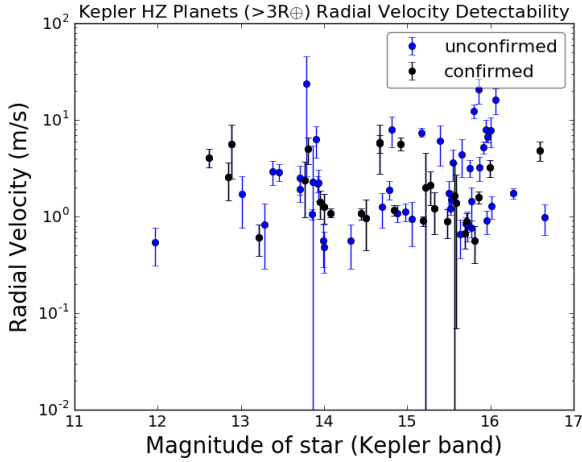


Figure 12. We plot the Kepler magnitude of the host star of both the unconfirmed and confirmed HZ planets and their expected radial velocity signatures to determine the expected detectability of these planets. We find that a large majority of the planets in our list have an estimated radial velocity semi amplitude between 1 and 10 m/s. As the *Kepler* telescope was focused on a field faint stars, the planets listed are at the limit of the capabilities of current RV detection instruments. Future radial velocity missions to follow up on these candidates should focus on those found closest to the top left corner of the graph, where the brightest stars host candidates with large RV semi amplitudes.

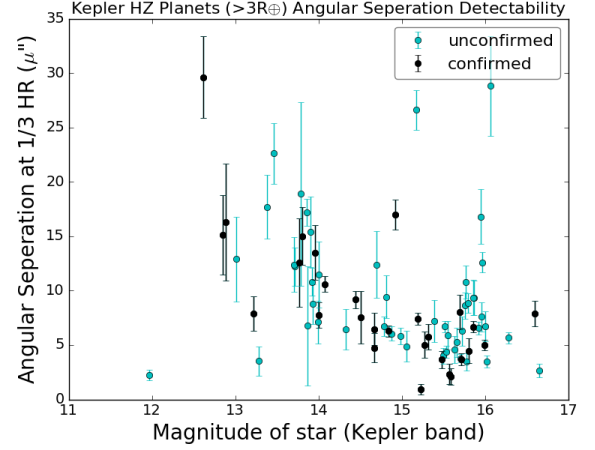


Figure 13. We plot the Kepler magnitude of the host star of both the unconfirmed and confirmed HZ planets and their expected Angular separation to determine the expected detectability of these planets. Confirmed candidates are noted by black dots and unconfirmed candidates by teal dots. Note the Y axis is the angular separation at $\frac{1}{3}$ Hill radius which we have taken as the typical distance of a stable moon. Future imaging missions will need the capabilities to resolve a separation between 1 - 35 μ arc seconds.

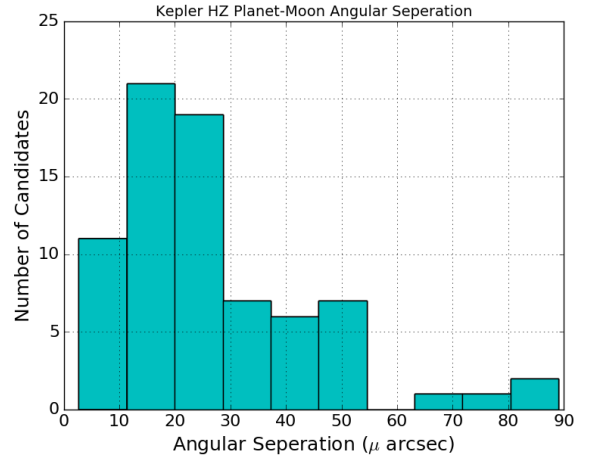


Figure 14. Here we show the distribution of Kepler habitable zone planets ($> 3R_{\oplus}$) Planet - Moon angular separation, with moons positioned at the full Hill radii. Potential moons of giant planets found in the habitable zone will likely have a maximum angular separation from their host planet between 1 - 90 μ arc seconds. This information can be used for planning of imaging future missions if we assume Kepler candidates are representative of the entire population of stars and planets.

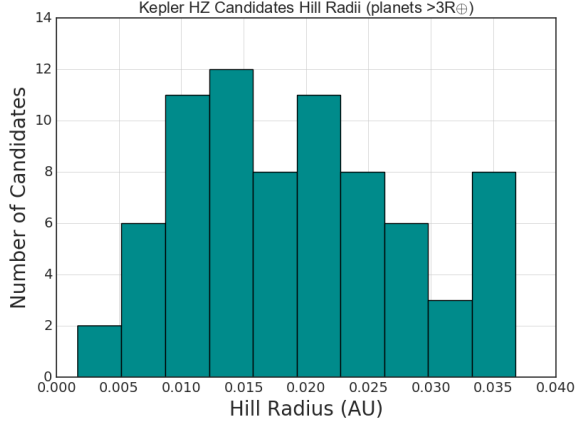


Figure 15. Here we show the distribution of Kepler habitable zone planets ($> 3R_{\oplus}$) Hill radii. Potential moons of giant planets found in the habitable zone will likely have a maximum radius of gravitational influence between 5 - 35 milli AU. This information can be used for planning of imaging future missions as the Kepler candidates can be considered representative of the entire population of stars.

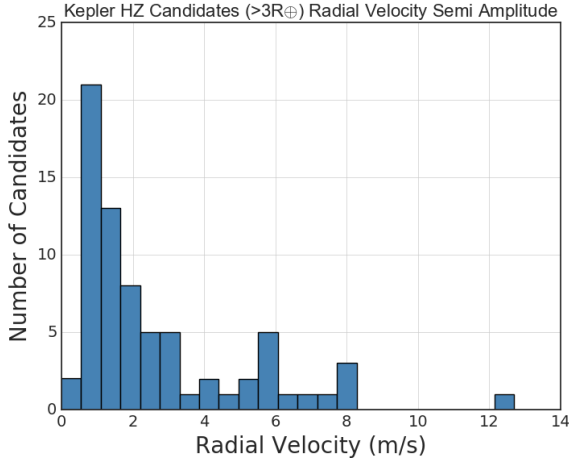


Figure 16. Here we show the distribution of Kepler habitable zone candidates ($> 3R_{\oplus}$) estimated radial velocity semi amplitudes. As the giant planets we are investigating reside in the habitable zone of their star, the increased distance from the host star produces a relatively small RV semi amplitude, thus the majority of the candidates have estimated radial velocity semi amplitudes of < 2 m/s.

a maximum radius of gravitational influence between 5 - 35 Milli AU. If we assume a similar distribution exists around the entire population of giant planets found in the HZ, we can use this information to calculate the expected angular separation of a moon around the closest giant HZ planets. This can then be used for planning of future imaging missions.

Finally, Figure 16 shows the distribution of the radial velocity semi amplitude of the HZ candidates. While we estimate the majority of candidates will have a signature < 2 m/s, there are a number of planets that are likely to have significantly larger signatures and thus more easily detectable. However, as the Kepler stars are faint, even the largest of these signatures are on the limit of our current detection capabilities and so these planets will still be difficult to observe. Note this graph does not take into account the separate calculations of the radial velocity semi amplitude for those planets $\geq 10R_{\oplus}$.

5. DISCUSSION AND CONCLUSIONS

From our calculations in Section 3 we found the frequency of giant planets ($R_p = 3.0\text{--}25 R_{\oplus}$) in the OHZ is $(6.5 \pm 1.9)\%$ for G stars, $(11.5 \pm 3.1)\%$ for K stars, and $(6 \pm 6)\%$ for M stars. For comparison, the estimates of occurrence rates of terrestrial planets in the HZ for G-dwarf stars range from 2% (Foreman-Mackey et al. 2014) to 22% (Petigura et al. 2013) for GK dwarfs, but systematic errors dominate (Burke et al. 2015). For M-dwarfs, the occurrence rates of terrestrial planets in the HZ is $\sim 20\%$ (Dressing & Charbonneau 2015). Therefore, it appears that the occurrence of large terrestrial moons orbiting giant planets in the HZ is less than the occurrence of terrestrial planets in the HZ. However this assumes that each giant planet is harboring only one large terrestrial exomoon. If giant planets can host multiple exomoons then the occurrence rates of moons would be comparable to that of terrestrial planets in the HZ of their star, and could potentially exceed them.

The calculations in Tables 3, 4 and 5 are intended for the design and observing strategies of future RV surveys and direct imaging missions. We found that a large majority of the planets in our list have an estimated RV semi-amplitude between 1 and 10 m/s. While currently 1 m/s RV detection is regularly achieved around bright stars, the *Kepler* telescope was focused on a field faint stars, thus the planets included in our tables are at the limit of the capabilities of current RV detection. Precision RV capability is planned for the forthcoming generation of extremely large telescopes, such as the GMT-Consortium Large Earth Finder (G-CLEF) designed for the Giant Magellan Telescope (GMT) (Szentgyorgyi et al. 2016), further increasing the capabilities towards the measurement of masses for giant planets in the HZ. Future RV surveys to follow up these candidates should focus on those candidates with the largest estimated RV semi-amplitudes orbiting the brightest stars.

Tidally heated exomoons can potentially be detected in direct imaging, if the contrast ratio of the satellite and the planet is favorable (Peters & Turner 2013). This is

particularly beneficial for low mass stars, where the low stellar luminosity may aid in the detection of a tidally heated exomoon. However, the small inner working angle for low-mass stars will be unfavorable for characterization purposes.

A new approach was proposed for detection and characterization of exomoons based on spectroastrometry (Agol et al. 2015). This method is based on the principle that the moon outshines the planet at certain wavelengths, and the centroid offset of the PSF (after suppressing the starlight with either a coronagraph or a starshade) observed in different wavelengths will enable one to detect an exomoon. For instance, the Moon outshines Earth at $\sim 2.7 \mu\text{m}$. Ground-based facilities can possibly probe the HZs around M-dwarfs for exomoons, but large space-based telescopes, such as the 15m class LUVOIR, are necessary for obtaining sharper PSF and resolving the brightness.

If imaging of an exomoon orbiting a Kepler giant planet in the habitable zone is desired, instruments must have the capability to resolve a separation between $\sim 1 - 90 \mu$ arcseconds. The large distance and low apparent brightness of the Kepler stars makes them unideal for direct imaging. But if we assume the distribution of Hill radii (Figure 15) calculated to surround the Kepler giant HZ planets to be representative of the larger giant HZ planet population, then our closest giant HZ planets could have exomoons with angular separations as large as $\sim 1 - 35 m$ arcseconds (assuming the closest giant HZ planets to reside between 1-10pc away).

Additional potential for exomoon detection lies in the method of microlensing, and has been demonstrated to be feasible with current survey capabilities for a subset of microlensing events (Liebig & Wambsganss 2010). Furthermore, the microlensing detection technique is optimized for star-planet separations that are close to the snow line of the host stars (Gould et al. 2010), and simulations of stellar population distributions have shown that lens stars will predominately lie close to the near-side of the galactic center (Kane & Sahu 2006). A candidate microlensing exomoon was detected by Bennett et al. (2014), suggested to be a free-floating exoplanet-exomoon system. However, issues remain concerning the determination of the primary lens mass and any follow-up observations that would allow validation and characterization of such exomoon systems.

There is great habitability potential for the moons of giant exoplanets residing in their HZ. These potentially terrestrial giant satellites could be the perfect hosts for life to form and take hold. Thermal and reflected radiation from the host planet and tidal effects increase

the outer range of the HZ, creating a wider temperate zone in which a stable body may exist. There are, however, some caveats including the idea that giant planets in the HZ of their star may have migrated there (Lunine 2001; Darriba et al. 2017). The moon of a giant planet migrating through the HZ may only have a short period in which the moon is considered habitable. Also, a planet that migrates inwards will eventually lose its moon(s) due to the shrinking Hill sphere of the planet (Spalding et al. 2016). Thus any giant planet that is in the HZ but still migrating inwards can quickly lose its moon as it moves closer to the host star.

(Sartoretti & Schneider 1999) uncovered another factor potentially hindering the detection of these HZ moons when they found that multiple moons around a single planet may wash out any transit timing signal. And the small radius combined with the low contrast between planet and moon brightness mean transits are also unlikely to be a good method for detection.

The occurrence rates calculated in Section 3 indicate a modest number of giant planets residing in the habitable zone of their star. Once imaging capabilities have improved, the detection of potentially habitable moons around these giant hosts should be more accessible. Until then we must continue to refine the properties of the giant host planets, starting with the radial velocity follow-up observations of the giant HZ candidates from our list.

ACKNOWLEDGEMENTS

This research has made use of the NASA Exoplanet Archive and the ExoFOP site, which are operated by the California Institute of Technology, under contract with the National Aeronautics and Space Administration under the Exoplanet Exploration Program. This work has also made use of the Habitable Zone Gallery at hzgallery.org. The results reported herein benefited from collaborations and/or information exchange within NASA’s Nexus for Exoplanet System Science (NExSS) research coordination network sponsored by NASA’s Science Mission Directorate. The research shown here acknowledges use of the Hypatia Catalog Database, an online compilation of stellar abundance data as described in Hinkel14, which was supported by NASA’s Nexus for Exoplanet System Science (NExSS) research coordination network and the Vanderbilt Initiative in Data-Intensive Astrophysics (VIDA). This research has also made use of the VizieR catalogue access tool, CDS, Strasbourg, France. The original description of the VizieR service was published in A&AS 143, 23.

REFERENCES

- Agol, E., Jansen, T., Lacy, B., Robinson, T.D., Meadows, V. 2015, *ApJ*, 812, 1
- Akeson, R.L., Chen, X.; Ciardi, D., et al. 2013, *PASP*, 125, 930
- Barnes, J. W., O'Brien, D.P. 2002, *ApJ*, 575, 1087
- Bennett, D.P., Batista, V., Bond, I.A., et al. 2014, *ApJ*, 785, 155
- Burke, C.J., Christiansen, J.L., Mullally, F., et al. 2015, *ApJ*, 809, 8
- Cameron, A.G.W., Ward, W.R. 1976, Abstracts of the Lunar and Planetary Science Conference, 7, 120
- Canup, R.M., Ward, W.R. 2002, *AJ*, 124, 3404
- Chen, J., Kipping, D. 2016, *ApJ*, 834, 1
- Cumming, A., Butler, R.P., Marcy, G.W., et al. 2008, *PASP*, 120, 531
- Darriba, L.A., de Ela, G.C., Guilera, O.M., Brunini, A. 2017, *A&A*, 607, A63
- Diaz, R.F., Rey, J., Demangeon, O., et al. 2016, *A&A*, 591, A146
- Dittmann, J.A., Irwin, J.M., Charbonneau, D., et al. 2017, *Nature*, 544, 333
- Dressing, C., Charbonneau, D. 2013, *ApJ*, 767, 1
- Dressing, C., Charbonneau, D. 2015, *ApJ*, 807, 1
- Elser, S., Moore, B., Stadel, J., Morishima, R. 2011, *Icarus*, 214, 2, 357-365
- Foreman-Mackey, D., Hogg, D.W., Morton, T.D. 2014, *ApJ*, 795, 1
- Foreman-Mackey, D. Morton, T.D. Hogg, D.W., Agol, E., Schlkopf, B. 2016, *ApJ*, 152, 206
- Fressin, F., Torres, G., Charbonneau, D., et al. 2013, *ApJ*, 766, 2
- Gillon, M., Triaud, A.H.M.J., Demory, B.O., et al. 2017, *Nature*, 542, 456
- Gould, A., Dong, S., Gaudi, B.S., et al. 2010, *ApJ*, 720, 1073
- Hartmann, W.K., Davis, D.R. 1975, *Icarus*, 24, 4, 504-515
- Heller, R. 2012, *A&A*, 545, L8
- Heller, R., Barnes, R. 2013, *AsBio*, 13, 18
- Heller, R., Pudritz, R. 2013, *ApJ*, 806, 2
- Heller, R., Marleau, G.-D., Pudritz, R.E. 2015, *A&A*, 579, L4
- Hinkel, N.R., Kane, S.R. 2013, *ApJ*, 774, 27
- Hinkel, N.R., Timmes, F.X., Young, P.A., Pagano, M.D., Turnbull, M.C. 2014, *ApJ*, 148, 54
- Holt, T.R., Brown, A. J., Nesvorny, D., Horner, J., Carter, B. 2017, *ApJ*, submitted (arXiv:1706.01423)
- Howard, A.W., Marcy, G.W., Bryson, S.T., et al. 2012, *ApJS*, 201, 15
- Hsu, H.-W., Postberg, F., Sekine, Y., et al. 2015, *Nature*, 519, 207
- Kaltenegger, L., Sasselov, D. 2011, *ApJ*, 736, 25
- Kane, S.R., Sahu, K.C. 2006, *ApJ*, 637, 752
- Kane, S.R., Gelino, D.M. 2012, *PASP*, 124, 323
- Kane, S.R., Hill, M.L., Kasting, J.F., et al. 2016, *ApJ*, 830, 1
- Kasting, J.F., Whitmire, D.P., Reynolds, R.T. 1993, *Icarus*, 101, 108
- Kipping, D.M. 2009, *MNRAS*, 392, 181
- Kipping, D.M., Fossey, S.J., Campanella, G. 2009, *MNRAS*, 400, 398
- Kipping, D.M., Bakos, G.A., Buchhave, L., Nesvorn, D., Schmitt, A.R. 2012, *ApJ*, 750, 115
- Kipping, D.M., Hartman, J., Buchhave, L., et al. 2013, *ApJ*, 770, 101
- Kipping, D.M., Forgan, D., Hartman, J., et al. 2013, *ApJ*, 777, 134
- Kipping, D.M., Nesvorn, D., Buchhave, L., et al. 2014, *ApJ*, 784, 28
- Kipping, D.M., Schmitt, A.R., Huang, X., et al. 2015, *ApJ*, 813, 14
- Kivelson, M.G., Khurana, K.K., Russell, C.T., et al. 1996, *Nature*, 384, 537
- Koch, D.G., Borucki, W.J., Basri, G., et al. 2010, *ApJ*, 713, 2
- Kopparapu, R.K. 2013, *ApJL*, 767, 1
- Kopparapu, R.K. Ramirez, R., Kasting, J.F., et al. 2013, *ApJ*, 765, 131
- Kopparapu, R.K., Ramirez, R., Schottel-Kotte, J., et al. 2014, *ApJ*, 787, L29
- Liebig, C., Wambsganss, J. 2010, *A&A*, 520, A68
- Lunine, J.I. 2001, *PNAS*, 98, 809
- Morabito, L.A., Synnott, S.P., Kupferman, P.N., Collins, S.A. 1979, *Science*, 204, 972
- Ochsenbein F., Bauer P., Marcout J. 2000, *AAS Meeting Abstracts*, 143, 221
- Nesvorny, D., Alvarellos, J. L.A., Dones, L., Levison, H.F., 2003, *The Astronomical Journal*, 126, 398-429
- Peters, M.A., Turner, E.L. 2013, *ApJ*, 769, 2
- Petigura, E.A., Howard, A.W., Marcy, G.W. 2013, *PNAS*, 110(48), 19273-19278
- Pollack, J. B., Burns, J. A., Tauber, M. E. 1979, *Icarus*, 37, 587
- Porco, C. C., Helfenstein, P., Thomas, P. C., et al. 2006, *Science*, 311, 1393
- Rowan, D., Meschiari, S., Laughlin, G., et al. 2016, *ApJ*, 817, 104
- Sartoretti, P., Schneider, J. 1999, *A&AS*, 134, 553

- Scharf, C.A. 2006, ApJ, 648, 1196
- Spalding, C., Batygin, K., Adams, F.C. 2016, ApJ, 817, 1
- Spergel, D. 2015, NASA reports
- Szentgyorgyi, A., Baldwin, A., Barnes, S., et al. 2016, SPIE, 9908, 990822
- Teachey, A., Kipping, D.M., Schmitt, A.R. 2017, ApJ, 155, 1
- Williams, D.M., Kasting, J.F., Wade, R.A. 1997, Nature, 385, 234
- Wittenmyer, R.A., Endl, M., Cochran, W.D., et al. 2006, AJ, 132, 177
- Wittenmyer, R.A., Tinney, C.G., O'Toole, S.J., et al. 2011, ApJ, 727, 102
- Wittenmyer, R.A., Tinney, C.G., Butler, R.P., et al. 2011 ApJ, 738, 81
- Wittenmyer, R.A., Butler, R.P., Tinney, C.G., et al. 2016, ApJ, 819, 28
- Zechmeister, M., Kürster, M., Endl, M., et al. 2013, A&A, 552, A78
- Zollinger, R.R., Armstrong, J.C., Heller, R. 2017, MNRAS472, 1